1-1-2013

Single Crystal to Single Crystal Polymerization of a Columnar Assembled Diacetylene Macrocycle

Weiwei Xu
University of South Carolina

SINGLE CRYSTAL TO SINGLE CRYSTAL POLYMERIZATION OF A COLUMNAR ASSEMBLED DIACETYLENE MACROCYCLE

By

Weiwei Xu

Bachelor of Engineering

Jilin University, 2006

Submitted in Partial Fulfillment of the Requirements

For the Degree of Master of Science in

Chemistry and Biochemistry

College of Arts and Sciences

University of South Carolina

2013

Accepted by:

Linda S. Shimizu, Director of Thesis

Chuanbing Tang, Reader

Lacy Ford, Vice Provost and Dean of Graduate Studies

ACKNOWLEDGEMENTS

I would like to express my deep gratitude to Professor Shimizu, my research advisor, for her patient guidance, enthusiastic encouragement and useful critiques of this research work.

I would also like to thank Dr. Tang, for his advice and assistance in keeping my progress on schedule.

My grateful thanks are also extended to Dr. Greytak, for his help and suggestions in doing the conductivity test, to Pravin and Dr. Kumar, who helped me in conductivity measurements.

I would also like to extend my thanks to Dr. Mark D. Smith, who provided excellent crystal structures for this thesis.

Finally, I wish to thank my wife, Xueyang Li, for her support and encouragement throughout my study.

ABSTRACT

Organic tubular materials have attracted lots of attentions for their potential applications as nanoscale fluidic transport systems, specific ion sensors, molecular sieves and confined molecular reaction containers. While conjugated polymers, due to delocalized π electrons, exhibit interesting solar cells and sensors applications. In this thesis, we developed a conjugated polymer which combines the attributes of conjugated polymers with tubular materials, which should have great potential to work as a sensing material.

We reproduced and scaled-up the synthesis of a polymerizable macrocycle **1** that contains two rigidly separated diacetylene units. We found that, through hydrogen bonding, **1** can assemble into columnar crystals and can be polymerized under a single crystal to single crystal transformation process to afford porous polydiacetylene (PDA) crystals. We studied the assembly of the macrocycle **1** under different conditions to give three different crystalline forms and micro-phase crystals, and also investigated their subsequent polymerizations. The macrocycle assembly and polymerized materials were characterized by a variety of technique. Since the gas adsorption measurement exhibited PDA crystals still retained its porosity and the polymer should have ability to uptake suitable guest molecules, therefore the absorption of iodine for PDA crystals was investigated as well.

TABLE OF CONTENTS

LIST OF FIGURES

CHAPTER ONE

BACKGROUND AND SIGNIFICANCE

1.1 Introduction of organic tubular assemblies

Organic tubular materials are interesting due to their potential applications as nanoscale fluidic transport systems[1], specific ion sensors, molecular sieves[2] and confined molecular reaction containers[3]. In the last two decades, non-covalent weak interactions, typically hydrogen and coordinative bonds were investigated to construct tubular materials through self-assemble of small components. By using this supramolecular strategy, various organic tubular materials with different shapes, sizes and functionalities have been developed. In this chapter we are going to give a basic introduction of organic tubular assemblies and our work in developing macrocyclic molecules which can work as building blocks to form porous columnar structures. We are also going to introduce the significance of conjugated polymers and our research in developing a tubular polydiacetylene polymer.

The study of enzymes demonstrated that the reaction efficiency and selectivity could be enhanced when chemical reactions were processed in a confined system[4, 5]. However, the construction of the analogues of these nature confined environments through synthetic strategy has been challenging, and the study of covalently built molecular reaction flasks was mostly focused on cyclodextrins, carcerands, and

hemicarcerands[6-8]. In order to overcome the challenge in developing synthetic confined environments, supramolecular strategies were used to construct tubular materials.

There are four possible strategies that can be used to form self-assembled tubular structures. One strategy is the folding of two dimensional molecules into helical structure[9-11]. By assembling tape like molecules into cylindrical shapes is another strategy to obtain tubular materials[12]. Wedge-shaped molecules can also work as building blocks to form cylinders, through intermolecular interactions, wedge-like subunits self assemble to discs that could subsequently stack into tubular structures[14]. The fourth method for tubular structures is the stacking macrocyclic molecules on top of each other to form continuous tubes. The examples of these four strategies will be introduced as follows.

Figure **1.1a** shows an example of folding a two dimensional starting material into a helical structure[9-11]. This strategy creates a tubular cavity. Moore, Wolynes, and co-workers designed oligophenylacetylenes by attaching phenylacetylene subunits together in a *meta* relationship. The resulting oligomer forms a helixturn structure, and the helix conformation could be stabilized by solvophobically-drivenpacking between backbone phenyl rings. The approximate 120^{o} turn angle prevents a close packed core and creates tubular cavity in which guest molecules of complementary size and shape were shown to bind.

Another efficient approach to obtain organic tubular material is to link tape like molecules to form cylindrical shapes[12] (Figure **1.1b**). According to this strategy, Fujita's group reported a coordination nanotube which was synthesized from tape **1** and enPd$(NO_3)_2$. Two Py-Py -Py (Py = 3-pyridyl, Py = 3,5-pyridylene) units in tape **1**

coordinate with metal to form tubular structures, and in order to prevent unfavorable intramolecular coordination, rigid biphenylene spacer was used to link the Py-Py -Py units[13]. The yield of the desired tubular structure was increased significantly when **3** was used as template. The framework remained unchanged even after template molecules were removed through extraction. This indicated that the stable empty tube should be capable of binding suitable guest molecules. Fujita's group found that a small rod like guest, sodium biphenylcarboxylate (guest **5**), and a biphenyl tetraoxatetradecane guest molecule (guest **4**) that is similar to **3**, were also good guests for this cavity.

Tubular structures can also be prepared from the self-assembly of sector-shaped subunits[12] (Figure **1.1c**). Percec and co-workers reported a hexagonal columnar liquid-crystal obtained from self-assemble of wedge-shaped molecules[14]. Here, a gallate core provided hydrophilic wedge-shaped subunits, while the alkylated phenoxy groups gave subunits hydrophobic functionalities. These wedge-shaped molecules were shown to self-assemble into tubular structure. The column structure positions the hydrophilic groups toward one another in the center of the column.

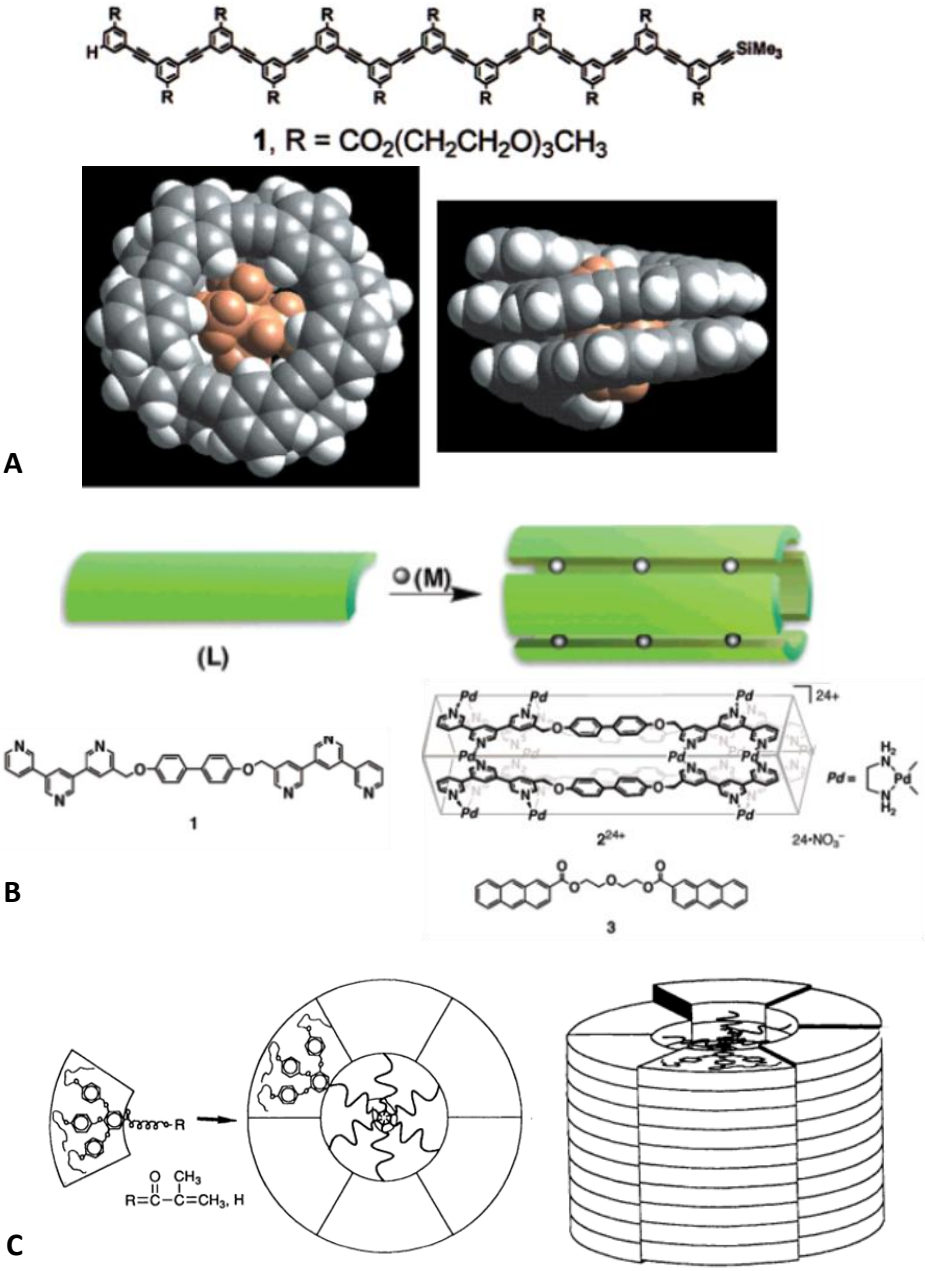

Figure 1.1. (a) Spacefilling model of the 1:1 complex of oligophenylacetylene and guest molecule viewed from the top and side. Reprinted with permission from ref. 11. Copyright (2000) American Chemical Society. (b) Organic nanotube obtained through self-assemble of tape like units. Reprinted with permission from ref. 13. Copyright (2004) American Chemical Society. (c) The tubular structure prepared from self-assemble of sector-shaped subunits.[14] Ref. 14 reproduced by permission of The Royal Society of Chemistry (RSC) on behalf of the Centre National de la Recherche Scientifique (CNRS) and the RSC

Self-assemble of macrocyclic molecules to form tubular or columnar structures are also a widely used motif to generate columns. For instance, Zhang and Moore examined the solid-state assembly of phenylacetylene macrocycle to a porous extended channel structures[36]. Ranganathan *et al.* also reported the assembly of less symmetric macrocycles with bisamide and bisurea groups[37, 38]. Our group developed bis-urea macrocycles as building blocks to form porous columnar assemblies (Figure **1.2a**). Urea contains both hydrogen bond donors and a hydrogen bond acceptor and readily forms directional intermolecular interactions. While there are several different ways of urea to interact with another urea group, the most common one is the three-centered interaction between the carbonyl group and two NHs from a neighboring urea. Through the three-centered interaction, bis-urea macrocycles designed in our group could stack with one another to form columns, and the dimensions of channel can be controlled by the size of spacers, which we used to synthesize the macrocycles (Figure **1.2b**).

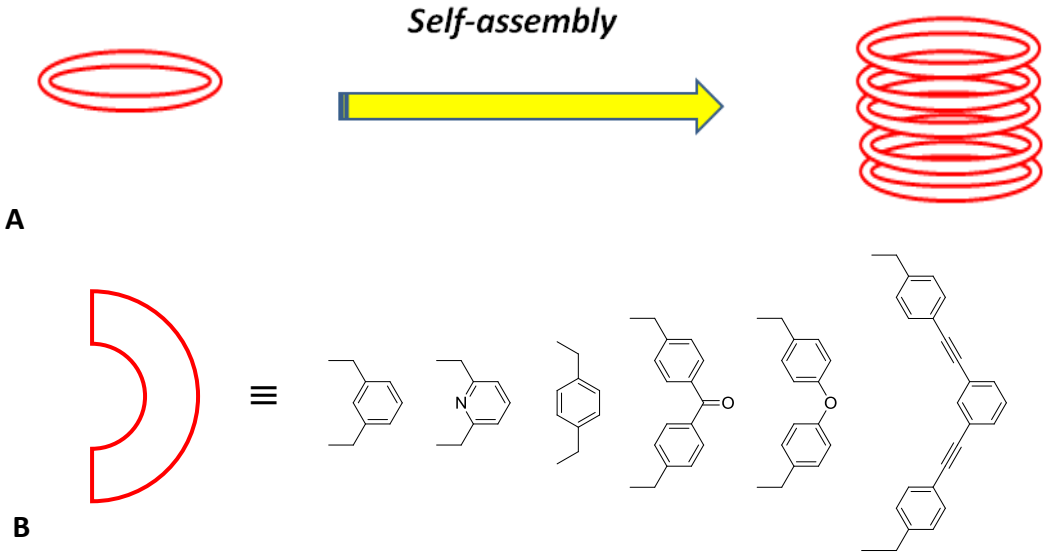

Figure 1.2. (a) Schematic representation of self-assembly of macrocyclic molecules. (b) different size spacers used to synthesize bis-urea macrocycles.

1.2 Background and Significance of Diacetylene Macrocycle

Polydiacetylenes (PDAs) can be easily synthesized by direct polymerization of prealigned diacetylene monomers. Since no initiators or catalysts are introduced into the polymerization process, purification is more straight-forward. Due to the conjugated structure, PDAs have a relative low band gap and the ability to carry electrons[15,16], and these properties afford PDAs potential applications in organic solar cells and sensors[17-20]. The most interesting property of PDA materials is their sensitivity to external stimulations. The absorption and emission spectra of PDA conjuated backbone can be easily changed by enviromental perturbations such as heat, mechanical stress, chemicals, and biological entities[21-23]. These optical changes are the basis of their use as both colorimetric and fluorescent sensors[24,25].

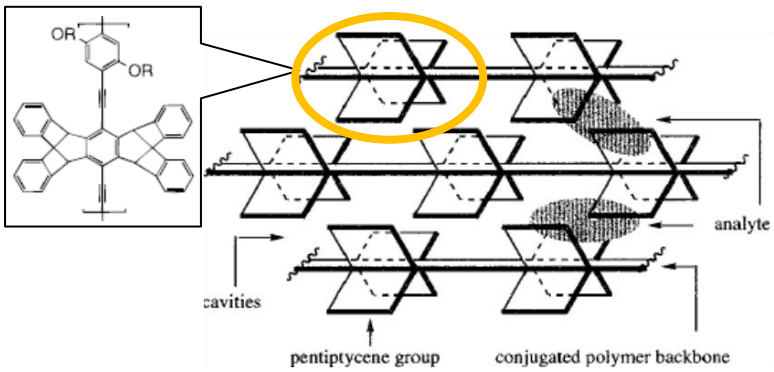

Figure 1.3. Scheme of porous conjugated polymer with three-dimensional pentiptycene. Reprinted with permission from ref. 26. Copyright (1998) American Chemical Society.

Although the solid-state (thin film) fluorescent sensory devices are required for many applications, the stability and the fluoresence quantum yields of most of solid-state sensors are very low, typically due to the formation of excimer and self-quenching. To resolve this problem, the Swager group incorporated pentiptycene into the polymer backbone[26]. This large steric group gave a porous structure (Figure **1.3**), which not only

enables the polymer to absorb guest molecules but also prevents the aggregation of polymer chains, and consequently increases the stablity and quantum yield of this material.[26]

The assembly of macrocyclic molecules through noncovalent interactions provides an alternate strategy for forming porous materials. The Shimizu group designed macrocycle **1** which consists of amides positioned in a *meta* relationship off a benzene as well as two diacetylene units attached to two sides of each amide, since diacetylene units are separated by macrocycle spacers, the aggregation of the corresponding PDA chains can be prevented. Hydrogen bonding of amide groups helps to guide the macrocycle into columnar structures to form porous crystals. UV irradiation or heat polymerizes the monomers to afford polymer (Figure **1.4**).

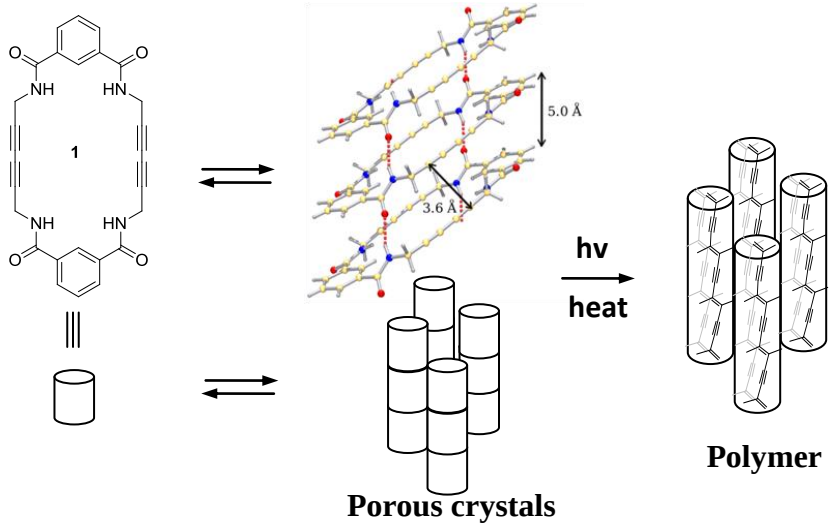

Figure 1.4. Monomer **1** assembles into columns that align the diacetylenes for polymerization through heat or light. The self-assemble and polymerization process is shown schematically

Macrocycle **1** was synthesized from isophthaloyl chloride and propargylamine to yield the acetylene amide intermediate in 80% yield. The cyclization step was processed by an Eglinton acetylene-acetylene coupling reaction[27,28]. Dr. Yuewen Xu optimized the cyclization reaction in DMSO and gave ~70% yield[29]. The first X-ray quality single crystals of macrocycle **1** were also obtained by Dr. Xu through slow evaporation of macrocycle **1** in 45:55:5 MeOH/CH_2Cl_2/H_2O (2 mg/mL). Macrocycle **1** stacked in columns with each individual cycle tilted at an angle of 41.6°. The monomer repeat distance was 4.98 Å, the distance of neighboring C1-C4 was 3.58 Å, which close to the optimal geometry for polymerization (Figure **1.4**)[30]. The shortest intercolumnar distance between the diacetylene units is ~ 6.2 Å, therefore, polymerization along the adjacent macrocycles is unlikely to occur. The polymerization reaction was initiated by heating monomers at 190 °C.

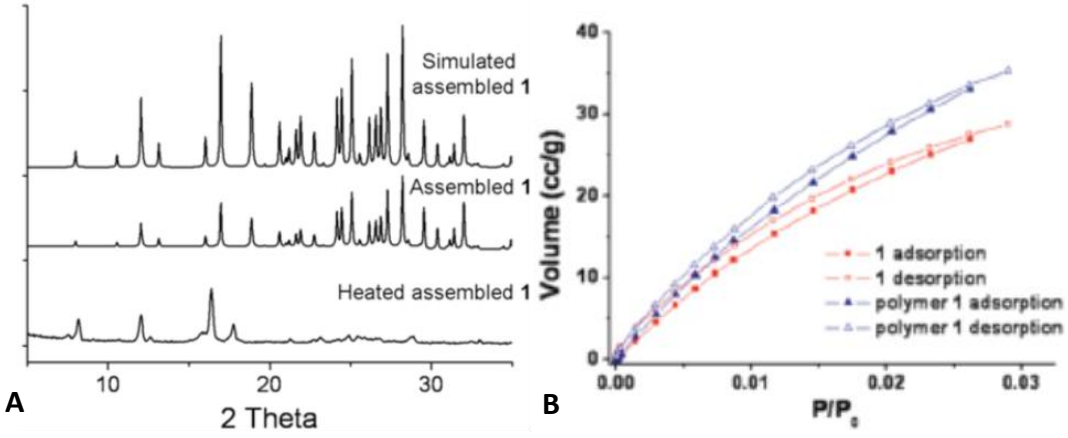

Figure 1.5. (a) PXRD patterns of assembled 1 and heat-treated 1. (b) CO_2 gas adsorption isotherms at 0 ℃ of assembled 1 and heat-treated 1 [29].

Thermally induced transitions of macrocycle was studied by differential scanning calorimetry (DSC), the DSC results indicated that the whole polymerization process gave a polymerization enthalpy of 250 kJ/mol, approximately twice that measured for a single diacetylene containing monomer (~150-165 kJ/mol) [30]. ^{13}C NMR, Raman and UV-vis were also run by Dr. Xu to do basic characterization of the heated sample. ^{13}C NMR showed the disappearance of diacetylene peaks (68-74 ppm) and the downfield shift of methylene peaks (29-32 ppm), which suggested the transformation of the monomer into polymer. Raman spectra also proved the formation of polymer. The original triple bond peak at 2081 cm^{-1} disappeared after heating and two new peaks were formed at 1147 and 2050 cm^{-1}, which assigned to the absorption of C=C and C≡C streting respectively. since the crystals were cracked after heating and not suitable for single crystal analysis, the PXRD was run to analyze the structure of PDA. The PXRD pattern of polymerized macrocycle **1** showed that the polymer retained a well-ordered crystalline structure (Figure **1.5a**). Gas adsorption measurements with CO_2 (g) at 0 ℃ (Figure **1.5b**) were used to test the porosity of assembled macrocycle **1**, which showed a type **I** isotherm and consistence with a microporous material. The calculated BET surface area of assembled macrocycle **1**was ~350 m^2/g. For the heated sample, a similar type **I** isotherm was observed with CO_2 (g) at 0 ℃, which displayed a slightly larger surface area (480 m^2/g), even though the internal channel must be quite small in diameter. The results of gas absorption experiment indicated that the polymerized sample still retained its porosity and the polymer should have ability to uptake suitable guest molecules. Our group has also observed crystals with no permanent cavity, which can expand like clays to absorb guests and gases[31, 32]. Others materials, such as *p-tert*-butylcalix[4arene developed by

Atwood's group has also absorbed uptake through seemingly close packed systems[33-35]. Thus, the uptake of gas in itself does not prove that the material has a permanent open pore.

In this chapter, we gave a brief summary on the organic tubular materials. We introduced four possible supramolecular strategies which can be used to construct tubular structures. Examples of these four strategies and our work in developing macrocyclic molecules which can work as building blocks to form porous columnar assemblies were shown in this chapter as well. We also introduced the significance of conjugated polymers and our research in developing tubular PDAs. In the next chapter, we are going to discuss the detail of the synthesis, assembly and subsequent single crystal to single crystal polymerization of diacetylene macrocycle.

1.3 Reference

(1) Eisenberg, B. *Accounts Chem Res* **1998**, *31*, 117.

(2) Borgnia, M.; Nielsen, S.; Engel, A.; Agre, P. *Annu Rev Biochem* **1999**, *68*, 425.

(3) Yoshizawa, M.; Klosterman, J. K.; Fujita, M. *Angew Chem Int Edit* **2009**, *48*, 3418.

(4) Sigler, P. B.; Xu, Z. H.; Rye, H. S.; Burston, S. G.; Fenton, W. A.; Horwich, A. L. *Annu Rev Biochem* **1998**, *67*, 581.

(5) Voges, D.; Zwickl, P.; Baumeister, W. *Annu Rev Biochem* **1999**, *68*, 1015.

(6) Vriezema, D. M.; Aragones, M. C.; Elemans, J. A. A. W.; Cornelissen, J. J. L. M.; Rowan, A. E.; Nolte, R. J. M. *Chem Rev* **2005**, *105*, 1445.

(7) Cram, D. J. *Science* **1983**, *219*, 1177.

(8) Cram, D. J. *Nature* **1992**, *356*, 29.

(9) Nelson, J. C.; Saven, J. G.; Moore, J. S.; Wolynes, P. G. *Science* **1997**, *277*, 1793.

(10) Prince, R. B.; Saven, J. G.; Wolynes, P. G.; Moore, J. S. *J Am Chem Soc* **1999**, *121*, 3114.

(11) Prince, R. B.; Barnes, S. A.; Moore, J. S. *J Am Chem Soc* **2000**, *122*, 2758.

(12) Bong, D. T.; Clark, T. D.; Granja, J. R.; Ghadiri, M. R. *Angew Chem Int Edit* **2001**, *40*, 988.

(13) Yamaguchi, T.; Tashiro, S.; Tominaga, M.; Kawano, M.; Ozeki, T.; Fujita, M. *J Am Chem Soc* **2004**, *126*, 10818.

(14) Percec, V.; Heck, J.; Tomazos, D.; Falkenberg, F.; Blackwell, H.; Ungar, G. *J Chem Soc Perk T 1* **1993**, 2799.

(15) Andrew, T. L.; Swager, T. M. *J Polym Sci Pol Phys* **2011**, *49*, 476.

(16) Yang, S. J.; Kertesz, M. *J Phys Chem A* **2006**, *110*, 9771.

(17) Chen, X.; Kang, S.; Kim, M. J.; Kim, J.; Kim, Y. S.; Kim, H.; Chi, B.; Kim, S. J.; Lee, J. Y.; Yoon, J. *Angew Chem Int Edit* **2010**, *49*, 1422.

(18) Tang, C. W. *Appl Phys Lett* **1986**, *48*, 183.

(19) Sariciftci, N. S.; Smilowitz, L.; Heeger, A. J.; Wudl, F. *Science* **1992**, *258*, 1474.

(20) Hoppe, H.; Egbe, D. A. M.; Muhlbacher, D.; Sariciftci, N. S. *J Mater Chem* **2004**, *14*, 3462.

(21) Okada, S.; Peng, S.; Spevak, W.; Charych, D. *Accounts Chem Res* **1998**, *31*, 229.

(22) Charych, D. H. *Science* **1993**, *261*, 1375.

(23) Yoon, J.; Chae, S. K.; Kim, J. M. *J Am Chem Soc* **2007**, *129*, 3038.

(24) Lee, J.; Yarimaga, O.; Lee, C. H.; Choi, Y. K.; Kim, J. M. *Adv Funct Mater* **2011**, *21*, 1032.

(25) Pindzola, B. A.; Nguyen, A. T.; Reppy, M. A. *Chem Commun* **2006**, 906.

(26) Yang, J. S.; Swager, T. M. *J Am Chem Soc* **1998**, *120*, 5321.

(27) Nantalaksakul, A.; Krishnamoorthy, K.; Thayumanavan, S. *Macromolecules* **2010**, *43*, 37.

(28) Coakley, K. M.; McGehee, M. D. *Chem Mater* **2004**, *16*, 4533.

(29) Xu, Y. W.; Smith, M. D.; Geer, M. F.; Pellechia, P. J.; Brown, J. C.; Wibowo, A. C.; Shimizu, L. S. *J Am Chem Soc* **2010**, *132*, 5334.

(30) Zhou, Q.; Carroll, P. J.; Swager, T. M. *J Org Chem* **1994**, *59*, 1294.

(31) Roy, K.; Wibowo, A. C.; Pellechia, P. J.; Ma, S. G.; Geer, M. F.; Shimizu, L. S. *Chem Mater* **2012**, *24*, 4773.

(32) Roy, K.; Wang, C.; Smith, M. D.; Dewal, M. B.; Wibowo, A. C.; Brown, J. C.; Ma, S. G.; Shimizu, L. S. *Chem Commun* **2011**, *47*, 277.

(33) Thallapally, P. K.; McGrail, B. P.; Dalgarno, S. J.; Schaef, H. T.; Tian, J.; Atwood, J. L. *Nat Mater* **2008**, *7*, 146.

(34) Thallapally, P. K.; Dobrzanska, L.; Gingrich, T. R.; Wirsig, T. B.; Barbour, L. J.; Atwood, J. L. *Angew Chem Int Edit* **2006**, *45*, 6506.

(35) Atwood, J. L.; Barbour, L. J.; Jerga, A.; Schottel, B. L. *Science* **2002**, *298*, 1000.

(36) Shetty, A. S.; Zhang, J. S.; Moore, J. S. *J Am Chem Soc* **1996**, *118*, 1019.

(37) Ranganathan, D.; Haridas, V.; Nagaraj, R.; Karle, I. L. *J Org Chem* **2000**, *65*, 4415.

(38) Ranganathan, D.; Haridas, V.; Gilardi, R.; Karle, I. L. *J Am Chem Soc* **1998**, *120*, 10793.

CHAPTER TWO

SINGLE CRYSTAL TO SINGLE CRYSTAL POLYMERIZATION OF A COLUMNAR ASSEMBLED DIACETYLENE MACROCYCLE

2.1 Abstract

Due to the extended π electron delocalization along their backbones, conjugated polymers exhibit interesting electric and optical properties for applications including light emitting diodes (LEDs)[1], photovoltaic cells[2], and sensors[3]. We developed a polymerizable macrocycle **1** that contains two diacetylene units, which are rigidly separated[4]. This chapter investigates the scale-up of the synthesis of macrocycle **1**. We found that **1** can assemble into columnar crystals and can be polymerized under a single crystal to single crystal transformation process to afford porous polydiacetylene (PDA) crystals. We investigated the assembly of the macrocycle **1** under different conditions to give different crystalline forms, and studied their subsequent polymerization. The macrocycle assembly and polymerized materials were characterized by a variety of techniques. We also examined the iodine doping of PDA crystals.

2.2 Introduction

Conjugated polymers, due to the delocalized π electrons, exhibit interesting electric and optical properties for various applications. Among those conjugated polymers, polydiacetylenes (PDAs) are unique in that they can be easily synthesized by direct polymerization of prealigned diacetylene monomers. This topochemical process was discovered by Wenger at around 40 years ago[5]. The polymerization of PDA appears to require reacting units to prealign precisely in repeat distance *d1* of ~4.9 Å, a neighboring C1-C4contact distance *d2* of 3.5 Å, and an orientation angle of 45 ° (Figure **2.1**).Then, the polymerization can be initiated by applying thermal treatment or photochemical energy.

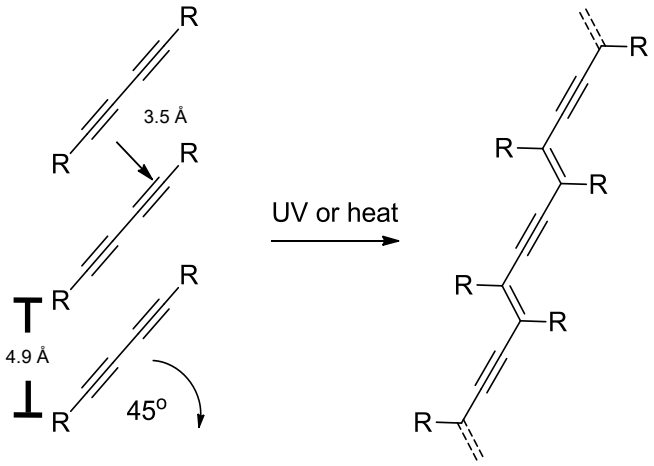

Figure 2.1. The ideal topochemical polymerization condition for polydiacetylene.

The conjugated structure of PDAs affords a relative low band gap (~2.0 ev) and the ability to carry electrons[6,7], which leads to their interesting applications in organic solar cells[2] and sensors[3]. The most attrative property of PDA materials arises from their enviromentally sensitive optical characteristics. The absorption and emission spectra of

the conjuated backbone can be easily changed by enviromental perturbations such as heat, mechanical stress, chemicals, and biological entities[8-10]. These optical changes are the basis of their use as both colorimetric and fluorescent sensors[11,12].

Supermolecular interations, sucn as hydrogen bonding, can provide methods to organize diacetylene monmers into assembly required for topochemical polymerization. Lauher's group found the oxalamides can crystallize with a spacing of 5 Å[13-15], which makes oxalamides as ideal host molecules to cocrystallize with diacetylene monomers, typically through hydrogen bonding, to build assemblies suitable for polymerization. By using this host-guest strategy, they developed a range of PDA polymers in perfect crystalline forms.

Figure **2.2a** shows oxalamide-diacetylene cocrystal obtained by Lauher's group[16]. Carboxylic acid form strong hydrogen bonding with pyridine groups on oxalamide substituent, together with the amide-amide hydorgen bonding, a cocrystal was construcuted by aligning the diacetylene monomer within ideal distance, and the crystal stucure of corresponding PDA polymer was also inverstigaed vis X-ray diffracttion. An DA-NTA (NTA = nitrilo triacetate) diacetylene amphiphile was reported by Gravel's group[17] (Figure **2.2b**). The diacetylene containing amphiphilic molecules can self-assemble into micelles with lipophilic C_{25} chains as core and nitrilo triacetic moieties as shell. Upon UV irradiation, the diacetylene units were polymerized and formed a stable micelle that can be used for biomedical applications, such as tumor image and drug delivery. PCDA **1** (Figure **2.2c**) reported by Cheng's group[18] can self-assembly into vesicles through hydrophobic interaction, diacetylene units in the vesicle were polymerized by UV irradiation, the resulting PDA vesicles exhibit blue to red phase

changes upon external stimulation, which gives it great potential in senor applications. Kim's group discovered that by changing the carboxylic acid head group of PCDA **1** to other functional groups changed the sensitivity of the polymer to external stimulation[19]. Thus, a series of diacetylene monomers with different head group moieties were synthsized by Kim's group to investigate the control of colorimetric reversibility of PDAs.

In general, great attentions has been put on polydiacetylenes for their application in microelectronics, sensors and biomendical areas. PDAs can be successfully achieved when the diacetylene monomers were prealigned using intermolecular interactions. Herein, we further investigated the macrocyclic diacetylene structure **1**, which was first reported and polymerized by Yuewen Xu[4]. In Yuewen's work, he optimized the syntheis of macrocyle **1**, generated the first crystal of assembled macrocyle **1** and investigated subsequent polymerization process of the crystal. Yuewen's work indicated that macrocycle **1** can be polymerized to give a poly or oligodiacetylene by heating. However, the large single crystals of macrocycle **1** obtained by Yuewen were splitted along their length during the heating, which were no longer suitable for the single crystal X-ray diffraction, thus Yuewen's initial communication only described the powder X-ray diffraction patterns of the product. In this chapter, we scaled up the synthesis of macrocyle **1** and sought to investigate the self-assembly of this macrocycle under different conditions and try to investigate if polymerization of this macrocyle can be carried out as a single-crysal to single-crystal process.

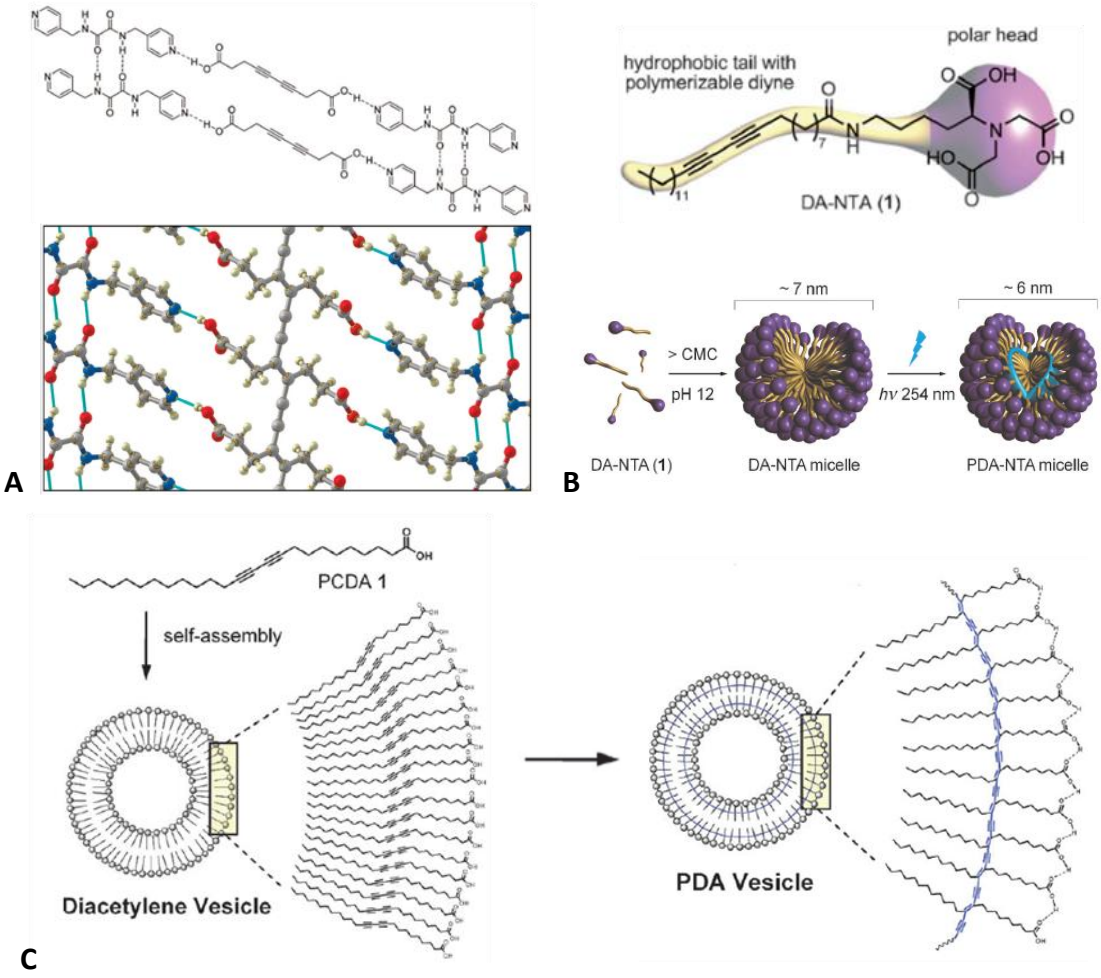

Figure 2.2. (a) Oxalamide-diacetylene cocrystal obtianed by Lauher's group. Reprinted with permission from ref. 16. Copyright (2005) American Chemical Society. (b) An DA-NTA (NTA = nitrilo triacetate) diacetylene amphiphile reported by Gravel's group. Copyright © 2012 WILEY-VCH Verlag GmbH & Co. KGaA, Weinheim (c) PCDA **1** self-assembly into vesicles through hydrophobic interaction. Copyright (2005) American Chemical Society.

2.3 Synthesis of Diacetylene Macrocycle 1

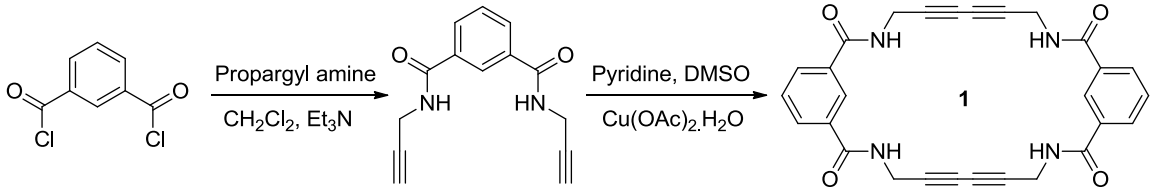

Scheme 2.1. Synthetic scheme of diacetylene macrocycle **1**

The diacetylene macrocycle **1** was synthesized as previously reported[4]. First, the commercial available isophthaloyl chloride and propargylamine were stirred with three equivalents triethylamine in dry methylene chloride to obtain the acetylene amide intermediate in 80% yield, which was identified by the chemical shift of acetylene protons at δ = 3.1 ppm. The key cyclization step was processed by an Eglinton acetylene-acetylene coupling reaction[20,21]. The disappearance of acetylene protons on NMR spectrum indicated the formation of the macrocycle. The cyclization reaction was optimized by Dr. Yuewen Xu and ran in DMSO in the air at room temperature. The crude product of cyclization reaction was purified through recrystallization to obtain crystals suitable for polymerization study and gave ~70% yield.

2.4 Structure Elucidation of Macrocycle 1 Crystals

2.4.1 Structure Information of Crystal I

The first type of single crystal of assembled macrocycle **1** (crystal **I**) was obtained through slow evaporation of macrocycle **1** in 45:55:5 MeOH/CH_2Cl_2/H_2O (conc. 2 mg/mL). We obtained numerous X-ray quality single crystals with structure identical to the prior reported structure. The type **I** crystal was first in white color but gradually

turned reddish after exposure to the light over several days. The color change of the crystal was presumably due to a small percentage of polymerization on the surface of the crystal, but which could not be detected by X-ray analysis. The X-ray analysis results of this crystal indicated that it had same crystal structure as the one reported by Dr. Yuewen Xu.

The X-ray analysis of a smaller crystal **I** (0.56 × 0.04 × 0.03 mm) with $C_{28}H_{20}N_4O_4 \cdot 2(H_2O)$ reveals that macrocycle **1** crystallized in the monoclinic P21/c space group with unit cell dimensions of 4.99 Å × 14.69 Å × 16.87 Å, and the volume of unit cell is 1226.89 $Å^3$. The asymmetric unit consists of half of one $C_{28}H_{20}N_4O_4$ molecule located on a crystallographic inversion center and one water molecule. Location and refinement of the water hydrogen atoms was problematic. Three electron density peaks near the water oxygen atom were clearly present in difference maps, in plausible positions for hydrogen atoms. Trial refinements indicated partial occupancy of two of the hydrogen positions, consistent with a water molecule disordered over two orientations. Hydrogen atoms bonded to carbon were located indifference maps before being placed in geometrically idealized positions and included as riding atoms. The nitrogen-bound hydrogen atoms were located in difference maps and refined freely.

Macrocycle **1** stacked into column with a repeat distance (*d1*) of 4.986 Å and a tilted angle of 45.7 °. The orientation angle of two adjacent cycles is 63.9 ° (Figure **2.3b**). The macrocycles self-assemble into columnar structure through amide-amide hydrogen bonding with N-(H)---O distance of 2.86 Å. There are two water molecules trapped in the cavity of each macrocycle, but the hydrogen bonding pattern of water molecules is not clearly defined because of disorder (Figure **2.3a**). Two sets of diacetylene units were

aligned along each side of column, the closest distance between acetylene groups on each side of ring is ~7.3 Å, the reacting carbon atoms of adjacent macrocycle have a contact distance (*d2*) around 3.6 Å. The supramolecular organization of the columnar assembled **1** is close to the ideal topochemical polymerization requirements[5]. The shortest intercolumnar distance between acetylene units is ~6.1 Å (Figure **2.3c**). Therefore, the polymerization along the adjacent column is unlikely to occur.

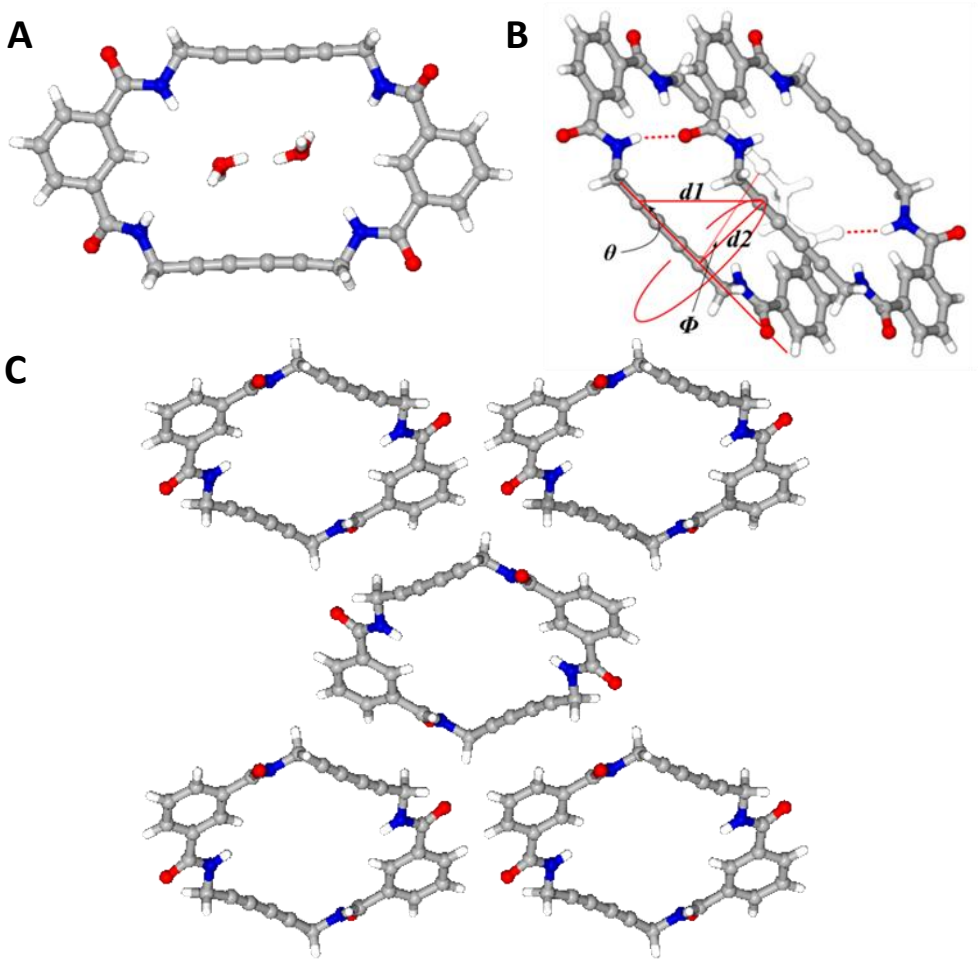

Figure 2.3. Molecular structure of crystal **I**. (a) Single diacetylene macrocycle **1** with two disordered water molecules incorporated. (b) Columnar assembly of macrocycle **1** viewed from side. The observed repeat distance *d1* of the assembly is 4.986 Å, the contact distance *d2* is 3.581 Å, the tilt angle θ is 45.7 ° and the orientation angle Φ is 63.9 °. (c) View down the column axis. Water molecules were removed for clarity.

2.4.2 Structure Information of Crystal II

The second crystalline form (Crystal **II)** was first found in solution that produced crystal **I**; however, after several days in ambient light, most of the crystals turned reddish in color, while a few developed into a darker color with a blue cast. The single crystal X-ray analysis of the red color crystal indicated it had structure identical to **I** type crystal of macrocycle **1**. The blue phase crystal was also subjected to the single crystal X-ray diffraction analysis, the approximate dimensions of the crystal was 0.04 ×0.03 × 0.03 mm^3, since the size of the crystal below the limitation of single crystal x-ray diffraction, the structure information of blue phase crystal was obtained by using synchrotron radiation.

The blue phase crystal (Crystal **II)** of macrocycle **1** with formula of $C_{28}H_{20}N_4O_4$•CH_3OH was crystallized in the triclinic P-1 space group, and gave a smaller unit cell with dimensions of 4.53 Å × 11.58 Å × 12.32 Å. The unit cell volume of type **II** crystal was 578.7 $Å^3$, which is approximately half the volume observed for crystal **I**. The asymmetric unit of crystal **II** consists of half of one disordered $C_{28}H_{20}N_4O_4$ cycle situated about a crystallographic inversion center and a fractionally populated, disordered solvent region which was modeled as methanol (Figure **2.4a**). The disorder of the cycle is caused by the presence of two opposite conformations of the amide group, which also affects the phenyl ring carbon C2-C7, and carbon atoms C12-C14 of the attached methylene and acetylene groups. The methanol guest incorporated in the macrocycle is disordered over two unique sites. Since the two unique methanol sites are located near an inversion center, four sites with total population 1.0 are generated for each macrocycle (Figure **2.4b**). Atoms affected by disorder were refined isotropically. Only the non-disordered atoms O1,

N1, C1, C9-C11 were refined with anisotropic displacement parameters. Hydrogen atoms were placed in geometrically idealized positions and included as riding atoms.

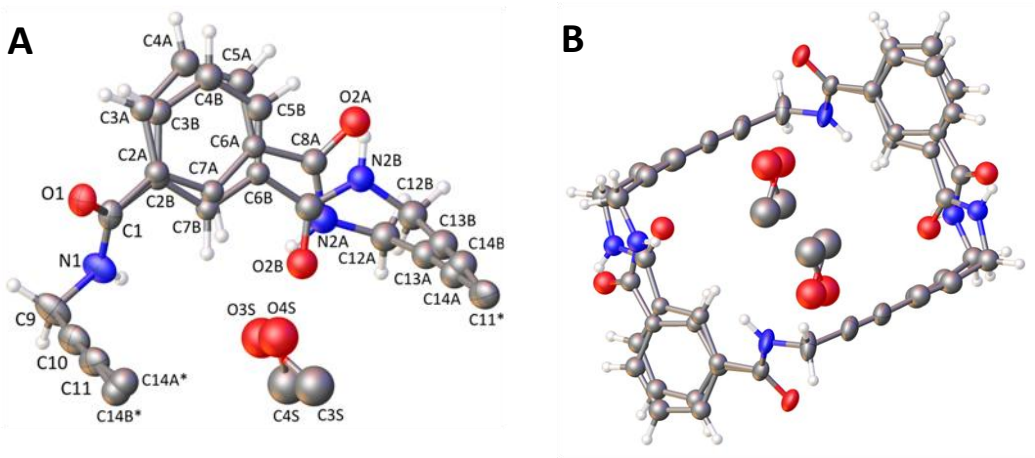

Figure 2.4. Molecular structure of crystal **II.** (a) Detail of the disorder of the cycle and methanol guests. Each disorder component has a population of 50%. The methanol guests are also disordered near an inversion center, only the independent components are shown. Displacement ellipsoids drawn at the 50% probability level. Only O1, N1, C1, C9-C11, which are not disordered, were refined anisotropically; disordered atoms were refined isotropically. (b) Single diacetylene macrocycle **1** with disordered MeOH incorporated. Total MeOH population = 1.0 MeOH per cycle.

The molecules of crystal **II** had a different conformation than the monoclinic crystal **I**. Unlike the flat structure of crystal **I**, the macrocycle plane in crystal **II** was folded, and the methylene carbons pivoted to two opposite directions. Due to the disorder of the amide functional groups, four possible conformers of macrocycle were given by the structure analysis, the major difference of four conformers came from the position of amide NHs. In conformer A (figure **2.5a**), the hydrogen of amide groups all pointed inward to the macrocycle center; in conformer B (Figure **2.5b**), N1(H) and N1*(H) pointed into the center of macrocycle, the other two NHs pointed outwards; in conformer C and D (Figure **2.5c,d**), there was only one NH pointed to the outside of macrocycle center, other three amide hydrogen pointed to inside. In each individual macrocycle, the

closest distance between acetylene groups on each side of ring is ~8.2 Å, which suggested that the cavity size of macrocycle was extended in crystal **II**.

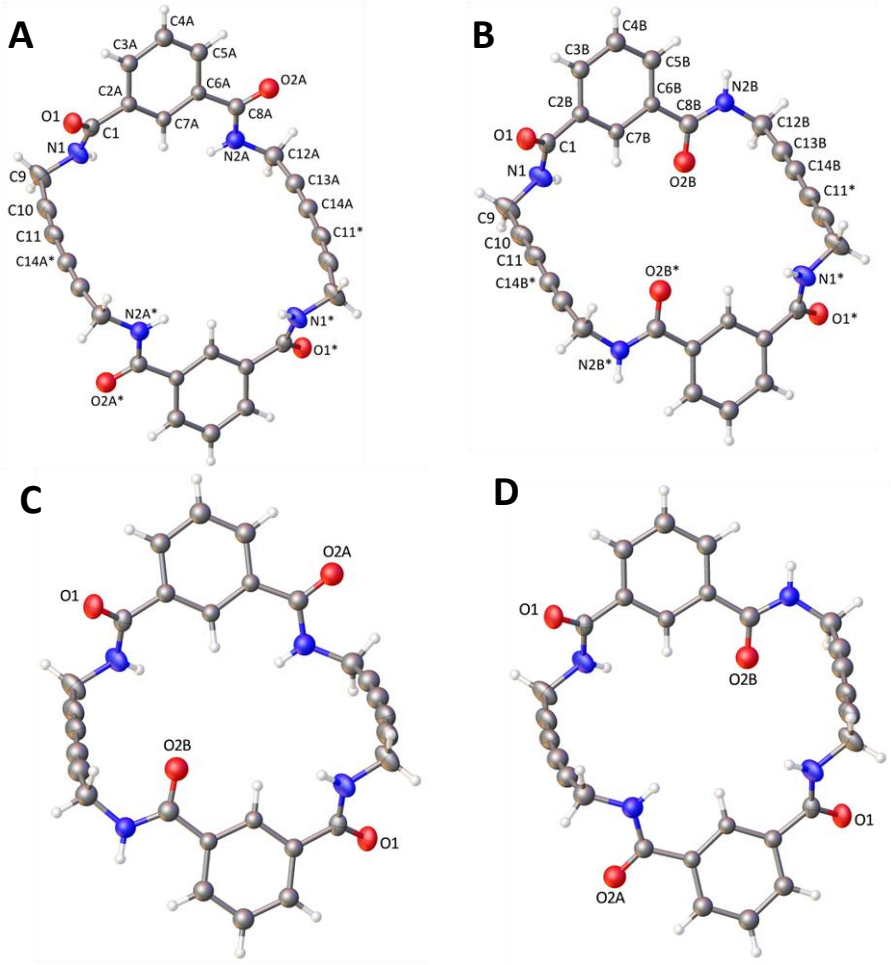

Figure 2.5. Four different conformations of the disordered macrocycle.

The molecules of triclinic crystal exhibited a different molecular conformation than the original monoclinic crystal, but they had similar stacking structure (Figure **2.6b**). The folded macrocycle also self-assembled into columnar structure through amide-amide hydrogen bonding, the N-(H)---O hydrogen bonding between the non-disordered amide groups, which defined tubular columns along the *a* axis direction (Figure **2.6b**). The N-

(H)---O distance of crystal **II** is 1.99 Å, which is shorter than crystal **I**. In crystal **II**, the macrocycle stacked with each individual cycle in a repeat distance *d1* of 4.585 Å, and the contact distance (*d2*) of the reacting carbon atoms is around 3.70 Å, still close to the structural parameters preferred for diacetylene polymerization[5], which indicated that the polymerization along the single column is likely to occur.

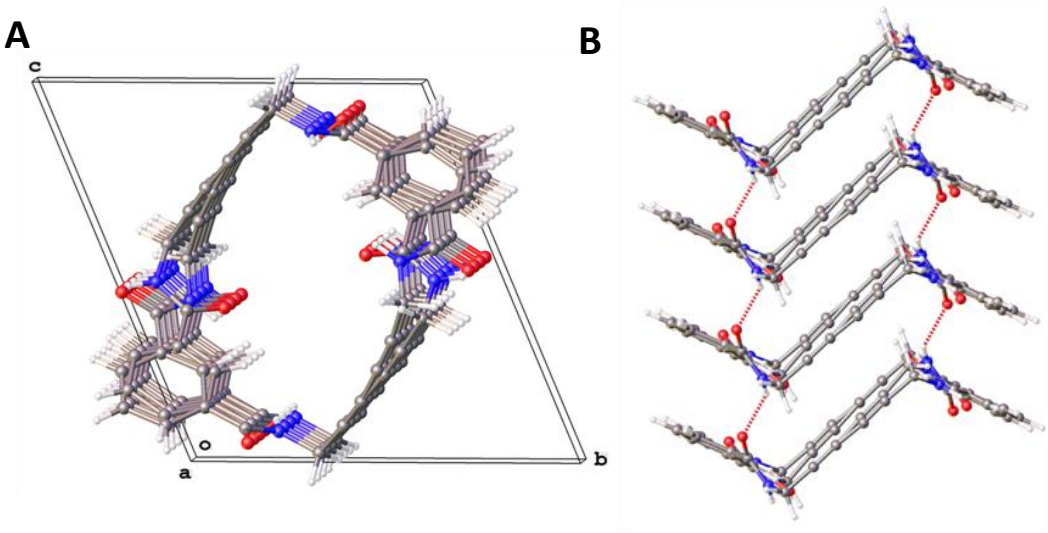

Figure 2.6. (a) The unit cell of crystal **II**, viewed down *a* axis. Unit cell with dimensions of 4.53 Å × 11.58 Å × 12.32 Å, the unit cell volume was 578.7 $Å^3$. (b) Columnar assembly of macrocycle **1** viewed from side. The observed repeat distance *d1* of the assembly is 4.585 Å, the contact distance *d2* is 3.702 Å. Disordered MeOH molecules were removed for clarity.

2.4.3 Structure Information of Crystal III

The third form of macrocycle **1** crystal (crystal **III**), colorless rods, was obtained by changing the ratio of the solvent system which crystal **III** grew from. Crystal **I** was yield through slow evaporation of macrocycle **1** in 45:55:5 MeOH/CH_2Cl_2/H_2O solution, the concentration of the solution was 2.0 mg/mL. The new crystalline form of macrocycle was also grown through slow evaporation technique, but by changing the ratio of the solvent components to 50:50:15 MeOH/CH_2Cl_2/H_2O, the concentration of macrocycle

was decreased into 1.0 mg/mL. The new crystals were of high quality, and the structure information of this new crystalline form was investigated by single crystal X-ray diffraction.

A type **III** crystal with size of $0.56 \times 0.08 \times 0.04$ mm^3 was subjected to the X-ray analysis. The XRD results suggested that macrocycle **1** crystallized in triclinic P-1 space group with an empirical formula of $C_{28}H_{20}N_4O_4 \bullet 4(H_2O)$. The asymmetric unit consists of half of one $C_{28}H_{20}N_4O_4$ cycle which is situated about a crystallographic inversion center, and two independent water molecules. Non-hydrogen atoms were refined with anisotropic displacement parameters. Hydrogen atoms bonded to carbon were placed in geometrically idealized positions and included as riding atoms. Hydrogen atoms bonded to nitrogen and oxygen were located in difference maps and refined isotropically.

The X-analysis indicated, unlike crystal **II**, macrocycle **1** gave a mostly planar structure in crystal **III**. There are four water molecules incorporated with each cycle (Figure **2.7a**). Two water molecules trapped in the cavity of macrocycle. The water molecules form hydrogen bonds with two amide groups on either side of the cycle. Another two water molecules are positioned on each side of the macrocycle plane: one lies on top and the other one on the bottom. The position of water molecules on either the side of macrocycle were fixed by O(H)---O hydrogen bonding with water molecules in the center of the macrocycle. The hydrogen of these two water also form the water-amide hydrogen bonds with adjacent macrocycles, which suggested that each macrocycle could link four other cycles, through the water tetramers, to build a 2D sheet structure (Figure **2.7b**). The 2D structures were formed parallel to the crystallographic (*bc*) plane (Figure **2.7d**).

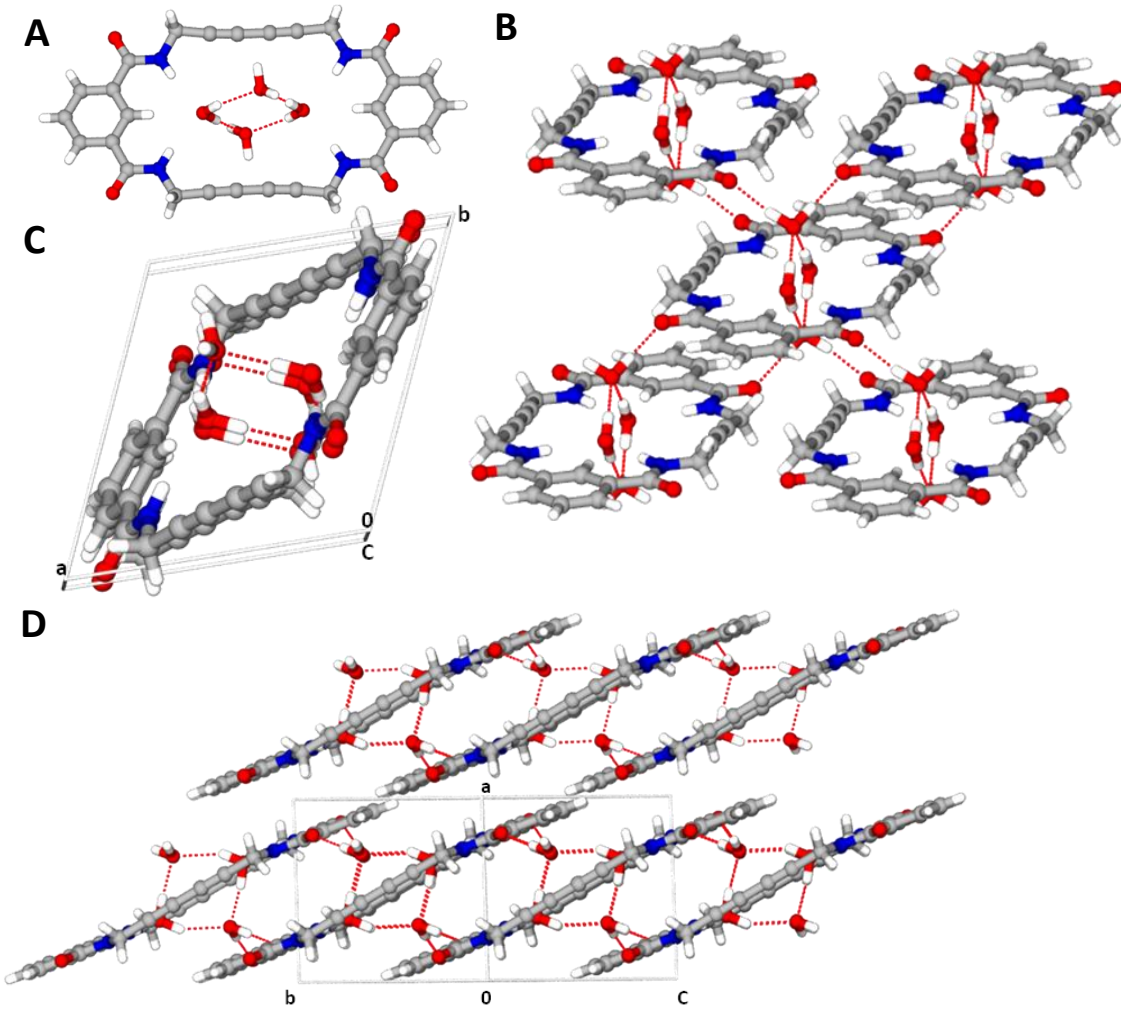

Figure 2.7. Molecular structure of crystal **III**. (a) Single diacetylene macrocycle **1** with four water molecules incorporated. (b) Five diacetylene macrocycles, the water tetramers link four other cycles into a 2D sheet structure. (c) Apparent column formed in crystal **III**, which viewed down the *c* axis. (d) 2D sheet structure built through hydrogen bonding packed parallel to the crystallographic (*bc*) plane.

Macrocycle also stacked to form columns in crystal **III**, but unlike the columnar structures of crystal **I** and **II** in which macrocycles are linked one by one through amide hydrogen bonds, there is no direct interaction between macrocycles. In this structure, the macrocycles are connected through hydrogen bonds with intervening water molecules, O(H)---O hydrogen bonding distance is ~1.86 Å (Figure **2.7b)**. Figure **2.7c** shows the

column was apparently formed along *c* axis, the X-ray results gave the unit cell dimensions of crystal **III** of 8.91 Å × 9.48 Å × 9.89 Å, and the unit cell volume is around 675.53 $Å^3$.

Still columnar like structures were formed in crystal **III**. The columns have a large offset (Figure **2.8a**), with respect to the column axis, the tilt angle θ of the macrocycle is 69.0 °. The contact distance (*d2*) of the acetylene carbon on adjacent cycle is 7.6 Å, a distance too large for diacetylene polymerization. Therefore, polymerization along the single column is unlikely to occur. The intercolumnar contact distance (C1-C4 distance) between acetylene units is ~4.2 Å (Figure **2.8b**), which is larger than the ideal diacetylene polymerization distance, suggesting that polymerization between columns is also unlikely to happen.

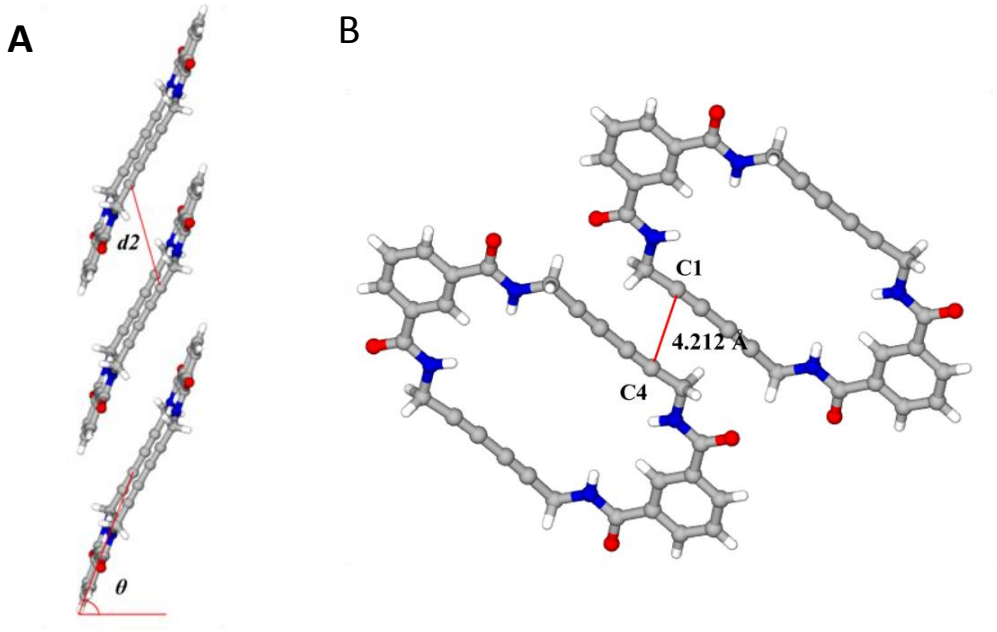

Figure 2.8. (a) The columns formed in crystal **III** have a large offset, with respect to the column axis, the tilt angle θ is 69.0 ° and the contact distance (*d2*) of the acetylene carbon on adjacent cycle is 7.6 Å. (b) Two adjacent diacetylene macrocycles with intercolumnar contact distance of 4.2 Å.

2.5 Study on Polymerization of Macrocycle 1

Our strategy to yield diacetylene polymer was to utilize self-assemble to preallign the macrocycles and then apply heat or UV irradiation to the macrocycle assembly to initiate the topochemical polymerization. Previous studies suggested that heating the macrocycle assembly at 190 ^{o}C for 12 h should efficiently complete the polymerization process. Although the UV irradiation could initiate the diacetylene polymerization, the UV-light may not penetrate deep into the bulk crystal of macrocycle. By using the Raman spectroscopy to examine the UV irradiated macrocycle **1** bulk crystal, we found some part of the crystal still not been polymerized, thus conversion of the polymerization reaction was low when it was carried out by UV irradiation method. Ideally, the polymerization process could occur on both side of the macrocycle to potentially form a porous conjugated polymer (Figure **2.9**). Dr. Yuewen Xu's work indicated that macrocycle **1** can be polymerized to give a poly or oligodiacetylene by heating.

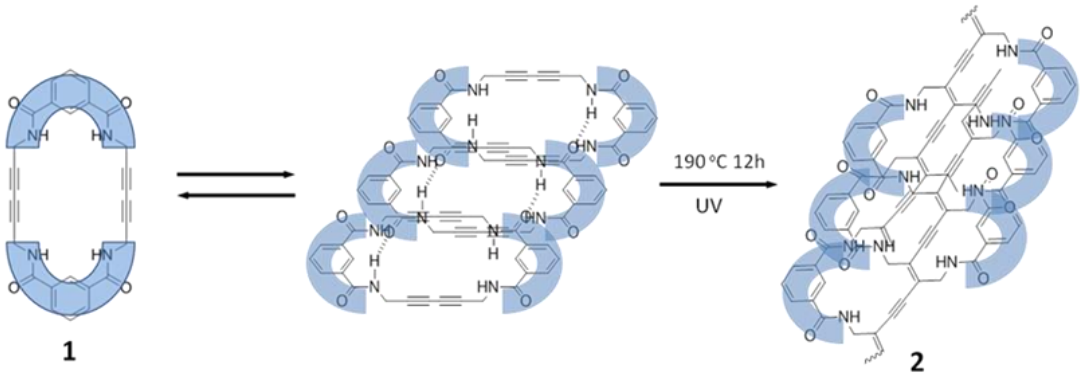

Figure 2.9. Schematic representation of self-assembly of diacetylene macrocycle **1**.Subsequent heating or UV-irradiation of the self-assembly afford PDA.

2.5.1 The Single Crystal to Single Crystal Polymerization of Type I Crystal

In type **I** crystals, the macrocycle **1** stacked into column with each individual cycle tilted at an angle of 45.7°. The reacting acetylene carbon atoms (C1,C4) of adjacent macrocycle have a contact distance (*d2*) of around 3.6 Å, which is close to the requirement of polymerization[5]. The predicted angle and contact distance requirements of topochemical polymerization was 45° and 3.5 Å. To determine if polymerization could occur in crystal **I**, single crystals were heated at 190 ^{o}C under inert atmosphere (N_2 gas) for 12 h. The crystals underwent a significant color change from reddish to dark brown, which is likely due to the formation of conjugated poly(ene-yne) structure that absorbs light at longer wavelengths. The product can also reflect light to give a metal like color (Figure **2.10**) and it is not soluble in any common solvents. The structure analysis was run for the thermal treated products. However, since the large single crystals were prone to splitting along their length during the heating, there were no longer suitable for the single crystal X-ray diffraction. Thus Yuewen's initial communication only described the powder X-ray diffraction patterns of the product.

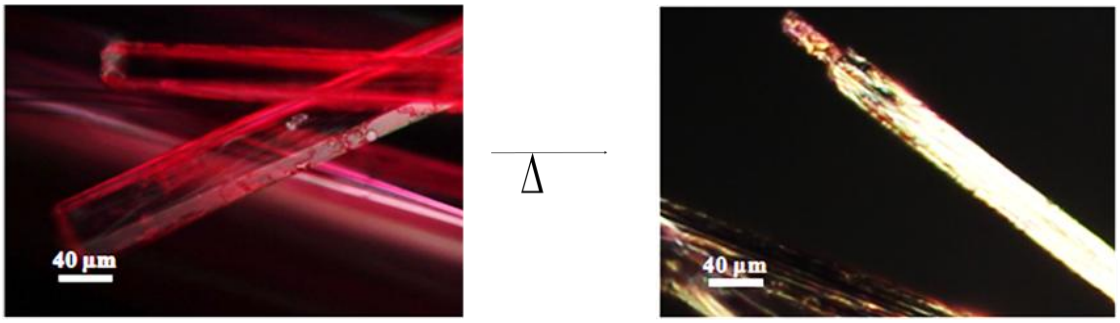

Figure 2.10. Microscope image of type **I** single crystals before and after heating.

Recently, I investigated the polymerization with smaller type **I** crystal, and observed a single crystal to single crystal polymerization to give a diacetylene polymer. The single crystal to single crystal nature of the transformation was verified by performing the X-ray intensity data collections before and after the thermal polymerization process using the same crystal (figure **2.11**). For data collection of the unheated sample, a smaller type **I** single crystal with dimensions of 0.52 × 0.05 × 0.04 mm^3 was selected, and the structure information of unheated crystal **I** was shown in Figure **2.11a**. After data collection and structure determination, the data crystal was removed from the diffractometer, placed on a glass slide and its position on the slide noted. The data crystal was then heated up to 190 ^oC under N_2 gas for 12 hours. When this process was completed, the glass slide and data crystal was returned to the X-ray lab and examined. The position of the crystal on the glass slide as well as the crystal shape appeared unchanged. Another data collection was performed on the heated crystal, and the structure was given in Figure **2.11b**. The single crystal-to-single crystal transformation occurs without a change in space group symmetry ($P2_1/c$ for both forms) or unit cell volume beyond a 9% contraction, the unit cell dimensions slightly changed from 4.99 Å × 14.69 Å × 16.87 Å to 4.90 Å × 14.59 Å × 16.29 Å. The unit cell volume correspondingly decreased from 1226.89 $Å^3$ to 1127.70 $Å^3$, which is primarily due to loss of the interstitial water molecule guests and the creation of hydrogen bonds between polymeric columns. The structural transition is therefore not accompanied by twinning.

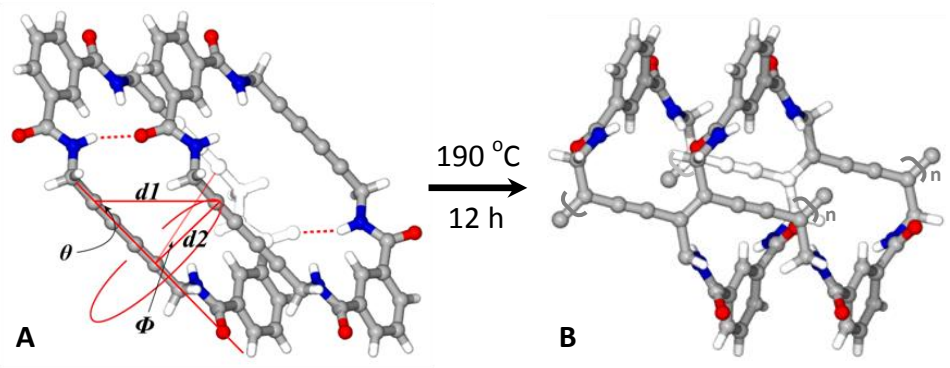

Figure 2.11. (a) Crystal structure of unheated diacetylene macrocycle **1** (type **I** crystal). The observed repeat distance *d1* of the assembly is 4.986 Å, the contact distance *d2* is 3.581 Å, the tilt angle θ is 45.7 ° and the orientation angle Φ is 63.9 °. Upon heating at 190 °C for 12 h the diacetylene macrocycles undergo a single crystal to single crystal polymerization process to afford polydiacetylene (b). Both structures were determined by the same single crystal.

The detail structure information of the diacetylene polymer (PDA) was given in Figure **2.12**. The thermally treated crystal (Figure **2.12a**) with empirical formula of $C_{28}H_{20}N_4O_4$ remains in the monoclinic $P2_1/c$ space group symmetry. The asymmetric unit of the PDA crystal consists of half of one polymeric formula unit, which is situated about a crystallographic inversion center. And the polymer crystal has a 1D columnar structure (inset of Figure **2.12b**). Figure 2b shows a top view of a single monomer unit imbedded in a polymer that runs the length of a single column. Compared to the monomer of the unheated crystal **I**, the monomer unit (figure **2.12b**) in the polymer was more folded due to the polymerization process and two water molecules, which previously incorporated in the cavity of each macrocycle, were removed during the thermal treatment. In the PDA monomer unit, the carbonyl oxygens O(1) and O(1)^{ii} point into the center of cycle and display intra-polymeric hydrogen bonds with amides from other two adjacent monomeric units within the same column (Figure **2.12c**). The N(2)H(2)---O(1) and N(2)^{ii}H(2)^{ii}---

$O(1)^{ii}$ distance is 2.86 Å. Since the monomer was folded during the polymerization process, the monomer unit in the PDA is no longer has a planar structure. Thus, it is easier to describe the PDA using a new cyclic repeat unit defined in Figure **2.12c**. The column built by the repeat of a new cycle. Each cycle (plane α) is linked by two poly(ene-yne) triple bonds on each sides. The new cycle in PDA consists of phenyl rings, amides and methylene groups of the original macrocycle connected through two carbon double bonds. The cavity size of PDA could be estimated by measuring the distance between two phenyl hydrogens which pointed into the center of the cycle and the distance between double bonds on either side, therefore the cavity dimension of PDA column was estimated to be 9 × 5 Å (center to center). Each column consists of a PDA polymer. These individual polymers are organized in three dimensions by a series of hydrogen bonds. Each polymeric column interacts with four other columns via hydrogen bonds that display N(1)H(1)---O(2) hydrogen bonds of 2.89 Å (Figure **2.12d**).

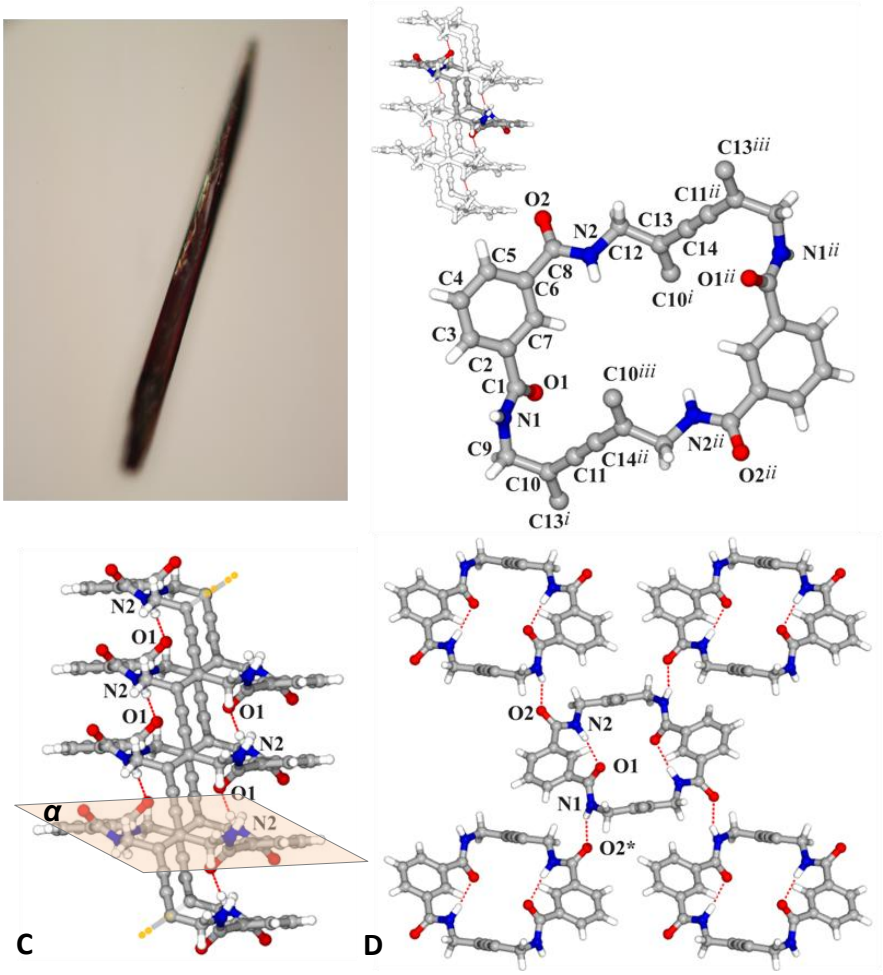

Figure 2.12. (a) Microscope image of polydiacetylene single crystal obtained via thermal treatment of macrocycle **1**. (b) One monomeric unit highlighted in the inset. Displacement ellipsoids drawn at the 60% probability level. (c) X-ray crystal structure of 1D columnar polydiacetylene. Intra-polymeric N(2)H(2)---O(1) hydrogen bonds shown as red dash lines. Bonds connected to non-shown neighboring monomeric units in the polymeric column were labeled as yellow dots. (d) Packing diagram of polymeric columns looking down from *a* axis. The columns are jointed via N(1)H(1)---O(2) hydrogen bonds.

To investigate the bond motion during the single crystal to single crystal transformation, crystal structure of both assembled **1** and polydiacetylene were juxtaposed in Figure **2.13** with the polymer structure on top and the monomer shown as the partially transparent structure behind. This analysis suggests that the major motion of

the monomer during the polymerization is due to the folding of macrocycle plane as the methylene carbons pivot. The C9-C10-C11 and C12-C13-C14 bond angle of assembled **1** was measured to be 177.1 ° and 173.6 ° respectively. Upon polymerization, the corresponding bond angles of polymer were shifted to 116.4 ° and 118.1 °. The repeat distance *d1* of adjacent cycle also contracted from 4.986 Å to 4.985 Å.

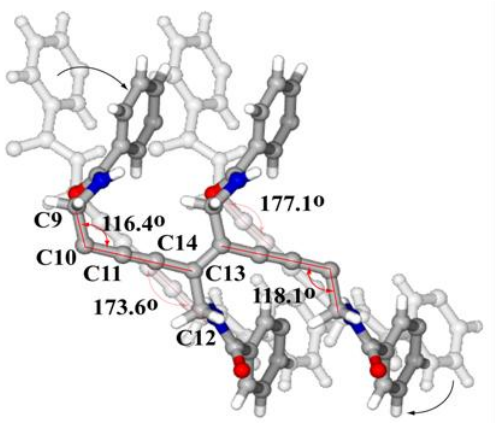

Figure 2.13. The background drawing shows the crystal structure of diacetylene monomer. The foreground drawing shows the structure of polydiacetylene. All the molecules were cut into half for clarity. The macrocycle rotated by a pivot of methylene carbons. The C9-C10-C11 bond angle changed from 177.1 ° to 116.4 °, C12-C13-C14 bond angle changed from 173.6 °to 118.1 °.

2.5.2 Basic Characterization of the Polymer (PDA)

UV-vis absorption spectra of the thermal treated type **I** crystals also gave evidence for the formation of the PDA. The adsorption of diacetylene macrocycle **1** in MeCN shown a sharp peak with λ_{max} = 208 nm. Since the polymer is insoluble in, we ground the polymer crystals into powder and made a PDA suspension in MeCN. Figure **2.14a** shows the UV-vis absorption spectra measured in MeCN suspension. No macrocycle monomer peak at 208 nm was observed. Instead, two broad absorption bands

were seen at λ_{max} = 571 nm and 620 nm which overlapped in the visible light range. The broad absorption band shown in Figure **2.14a** could be attributed to the presence of different length of PDA in our sample[22]. The formation of conjugated poly(ene-yne) chain of PDA should reduce the band gap of polymer and shift the UV-vis absorption of polymer to longer wavelengths.

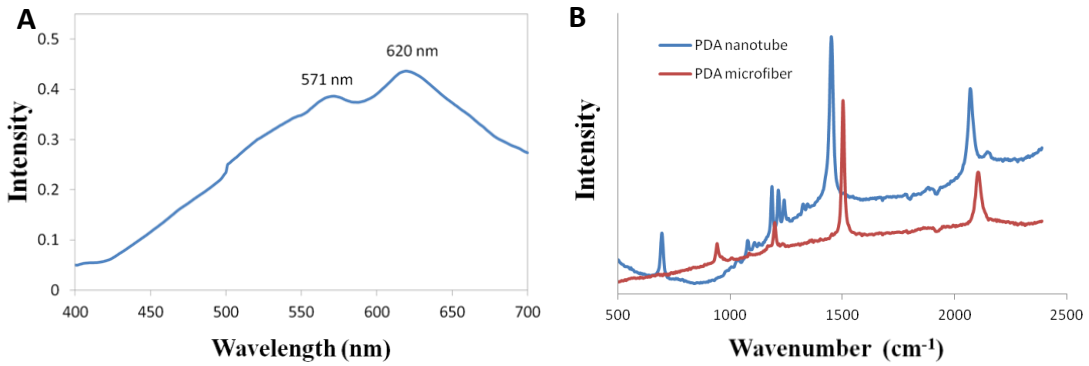

Figure 2.14. (a) UV-vis absorption spectra of PDA suspension in MeCN; (b) Raman spectra of PDA which obtained by thermal treatment of crystal **I,** and commercial available PDA-nanotube (Sterm Chemicals, Inc. Compound #06-1060).

Raman spectroscopy proved to be an efficient method to detect the double and triple bonds in PDA polymer. These unsaturated bonds usually have characteristic frequencies on the Raman spectra due to their distinctive stretch modes, for instance, C≡C bonds have frequencies in 2190-2300 and 2100-2140 cm^{-1} range, the stretch of C=C bonds usually found in 1600-1675 and 1580-1620 cm^{-1} range, while aromatic rings breathing normally located at 990-1010 cm^{-1}. Figure **2.14b** compares the Raman spectra of the PDA obtained by thermal treatment of crystal **I** (red line) to the commercial available PDA-nanotube reference (blue line) from Sterm Chemicals. The spectrum of

reference PDA-nanotube had two peaks located at 1450 and 2100 cm^{-1} area, which should attributed to the carbon double bond and triple bond stretch of the poly(ene-yne) chain of PDA. Similarly, the Raman spectrum of our PDA also had two main peaks observed at these two ranges. The peaks located at ~1506 and ~2107 cm^{-1} correspond to the stretch of double and triple bonds in PDA[23]. The peaks at ~941 cm^{-1} were assigned to the -CH deformation of aromatic ring, while the peak located at ~1200 cm^{-1} may come from the C-N stretch of the amide groups[24].

The insolubility of the heated material is typical for PDAs, and it hindered our characterization of the product. Hence, solid state ^{1}H-^{13}C COSY (HETCOR) was used to do further analyze to the material. According to Figure **2.15**, we observed that the heated product has broad peaks, which is more typical nature of polymers. In the ^{13}C NMR of heated sample, two significant chemical shifts were seen at 100-110 ppm, and no correlated chemical shifts were found in the corresponding proton NMR, thus these two peaks should be assigned to the newly formed C=C bonds. No non-polymerized acetylene peaks were observed in the ^{13}C spectrum, which indicated a high conversion of polymerization reaction. The ^{13}C single of $–CH_2$ was found at 44 ppm[25], compared with the chemical shift of methylene group in macrocycle **1** (29-32 ppm), the peak was downfield shifted by 14 ppm, which should be due to the transformation from methylene to conjugated allylic system during the polymerization process. Thus, the solid state ^{1}H-^{13}C COSY of thermally treated crystal **I** gave another strong evidence for the formation of the PDA.

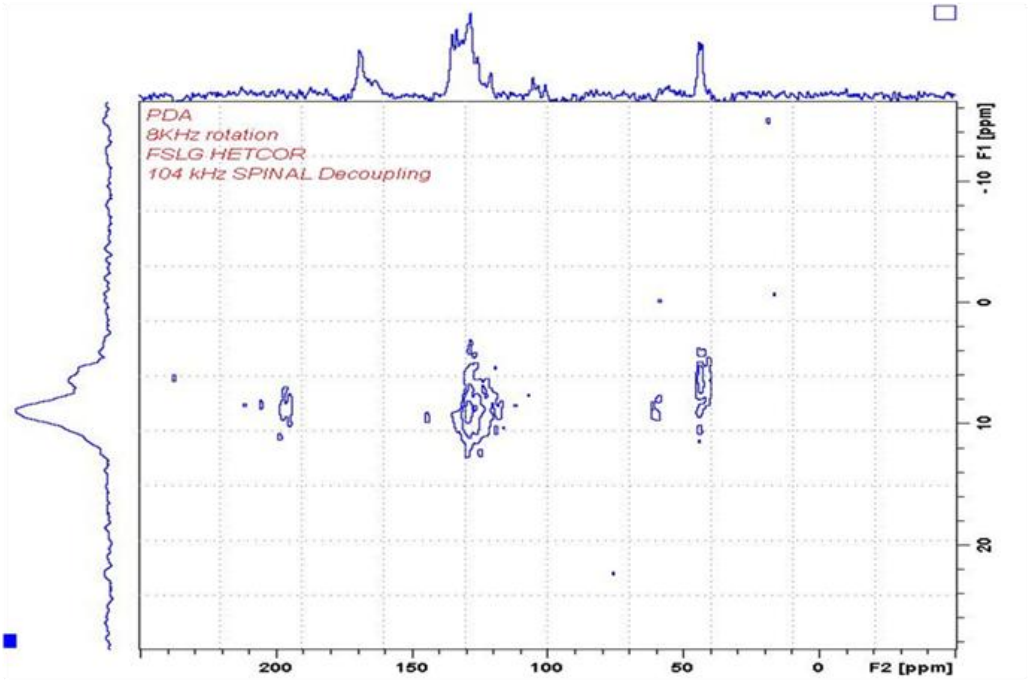

Figure 2.15. Solid state ^{1}H-^{13}C COSY (HETCOR) of PDA.

The Powder X-ray diffraction (PXRD) was used to probe the structure information of thermally treated type **I** crystals. The single crystal X-ray diffraction gave evidence of single crystal to single crystal transformation from crystal **I** to polydiacetylene. We turned to the PXRD to assess the purity and homogeneity of the bulk PDAs. The PDA crystals were ground into powder form and examined by PXRD (Figure **2.16**). The sharp peaks of the observed PXRD pattern indicated the bulk PDA crystals still retain well-ordered crystallinity. The PXRD pattern was also simulated from the coordinates of the PDA single crystal (Figure **2.16** blue line). Comparison of two patterns shows that the PDA bulk crystals closely match the simulated pattern and no additional peaks were observed. This suggests that there was only one phase crystal in the bulk crystals, and that the bulk PDA crystals have similar structure as the PDA single crystals. Through closely comparison of two patterns, it is apparent that several peaks are

absent in the observed pattern, including peaks at 19.2°, 21.5°, 22.3°, 27.1°, and 30.6°. The intensity of some peaks was also slightly different from simulated pattern. This difference may be due to the preferred orientation of the sample.

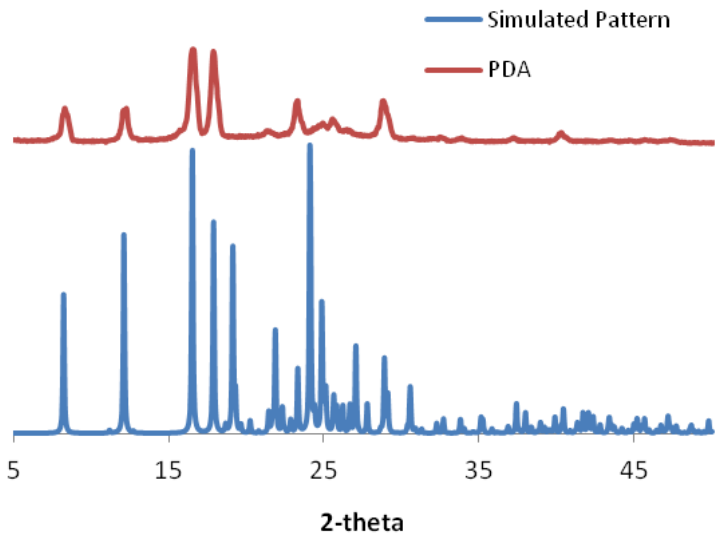

Figure 2.16. Observed powder X-ray diffraction (PXRD) pattern of bulk PDA crystals and simulated PXRD pattern calculated from PDA single crystal.

2.5.3 Study on Polymerization of Type II Crystal

In crystal **II**, the macrocycle stacked with each individual cycle in a repeat distance *d1* of 4.585 Å. The contact distance (*d2*) of the reacting carbon atoms is around 3.70 Å. The supramolecular organization of the columnar assembled **1** in crystal **II** is also close to the ideal topochemical polymerization requirements. Thus we tried to heat type **II** crystals at 190 °C under N_2 gas for 12 hours. Since the heated crystals no longer suitable for sing crystal X-ray diffraction, we used the powder X-ray diffraction to study the structure information of thermally treated type **II** crystals (Figure **2.17a**). Unlike

heated crystal **I**, the observed PXRD pattern of type **II** crystals only gave one broad diffraction band, which suggested that the type **II** crystals loss its crystallinity during the heating. The heated product was also examined by Raman spectroscopy (Figure **2.17b**). The peak appeared at ~1500 cm^{-1} provide the evidence for the formation of carbon double bonds[23], which suggested that diacetylene polymerization did occurred in type **II** crystals through heating; however, the crystalline structure was altered during this process. The solid state UV-vis absorption spectrum given in Figure **2.18** also suggests the formation of diacetylene polymer, and the broad band could attribute to the absorption of PDAs with different chain length[22].

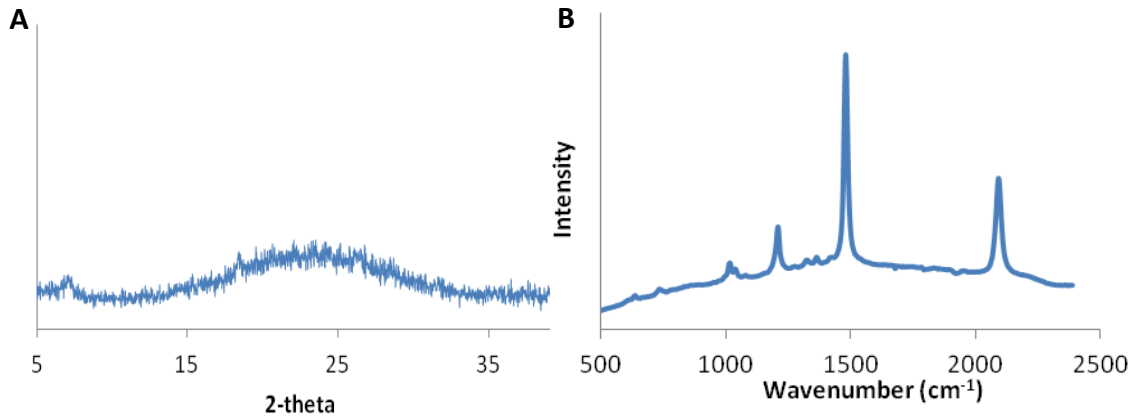

Figure 2.17. (a) Powder X-ray diffraction pattern and (b) Raman spectrum of heated type **II** crystal.

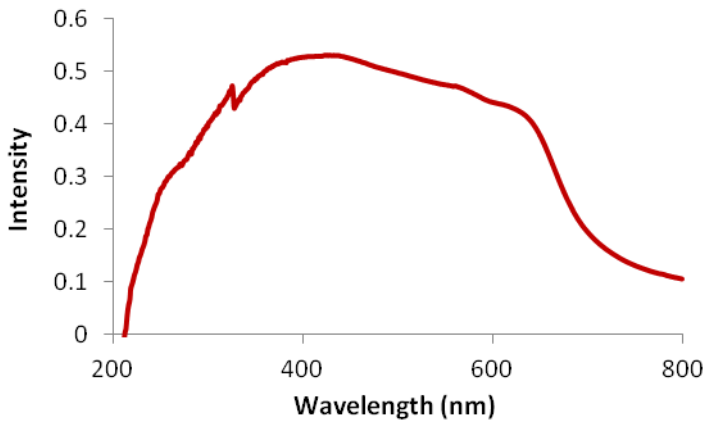

Figure 2.18. Solid state UV-vis absorption spectrum of heated type **II** crystal.

2.6 Study of Polydiacetylene Microcrystal

The conjugated structure of PDAs afford a relative low band gap (~2.0 ev) and the ability to carry electrons, which leads to their interesting applications in organic solar cells and sensors[3]. To explore these potential applications, polydiacetylenes are usually fabricated into one dimensional (fibers) or two dimensional (films or patterns) forms by different techniques, such as Electrospinning[26] (PDA fibers), Langmuir–Blodgett/Langmuir–Schaefer deposition[27-29] (PDA films), Molecular layer deposition[30] (PDA films), solvent casting (PDA films[31] and fibers[32]), and electrophoretic deposition[33] (PDA patterns). We investigated the assembly behavior of diacetylene macrocycle **1** by spin-coating on silica, glass, and quartz substrates, SEM and AFM were used to study the morphology of the corresponding polymer. Instead of forming two dimensional films, we obtained polydiacetylene microcrystals by spin-casting macrocycle solutions on these substrates.

2.6.1 Polydiacetylene Microcrystal Generated via Fabrication Condition Control

Polydiacetylene microcrystals were obtained using spin-coat technique. Micro-size crystals were assembled while spin-coating a macrocycle **1** solution (50:50 MeOH/CH_2Cl_2) on substrates. Further thermal treatment of macrocycle **1** microcrystals induced the polymerization process and afforded polydiacetylene microcrystals. We investigated different spin-coating factors, such as concentration of macrocycle solution, spin rate and time to find the optimal condition to obtain well distributed microcrystals. The desired polydiacetylene microcrystals were generated by spinning macrocycle solution with concentration of 1.0 mg/mL at a rate of 1000 rpm for 90s on silicon wafer. Figure **2.19a** shows the SEM image of these microcrystals, which has 1D needle like structures that were randomly disturbed over the surface. The normal distribution calculation gave an average length of microcrystal around 3 μm (Figure **2.19b**). Microcrystals generated at higher solution concentration (1.5 mg/mL) are shown in Figure **2.19c**, which have similar 1D structure but with larger average length of ~5 μm (Figure **2.19d**). This suggests that the size of polydiacetylene microcrystal can be controlled by the concentration of macrocycle **1** solution. The contact AFM scan of spin-coated sample gave the thickness of polydiacetylene microcrystal around 50 nm.

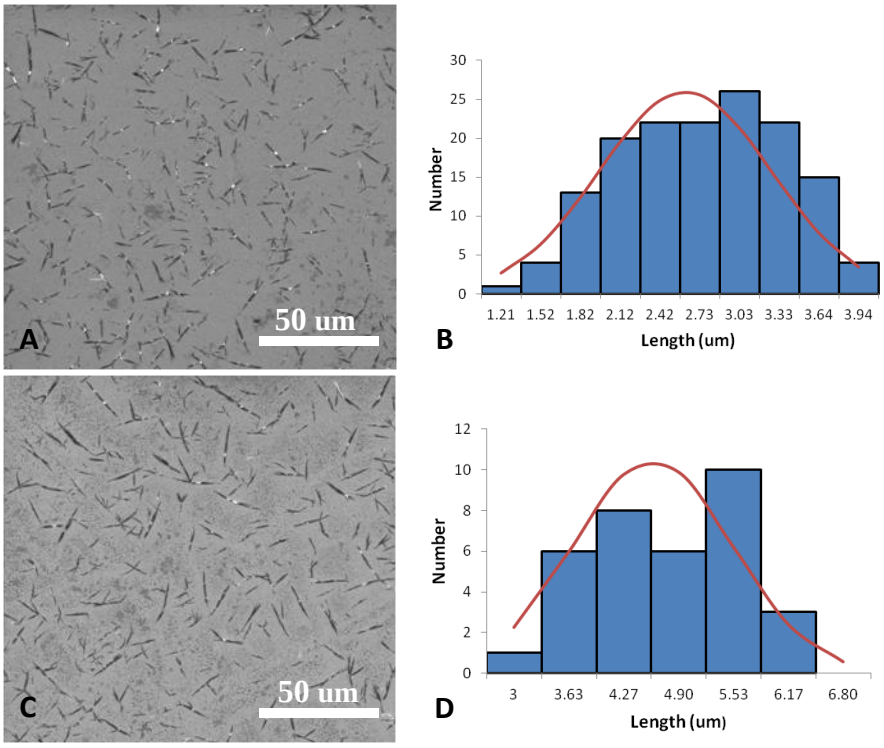

Figure 2.19. (a) SEM image of polydiacetylene microcrystal generated by spin coating 1.0 mg/mL macrocycle **1** solution on Si wafer at a spin-rate of 1000 rpm for 90 s, the spin coated sample was heated at 190 ^{o}C for 3 h to induce the polymerization. (b) Size distribution calculated based on microcrystal in (a). (c) SEM image of polydiacetylene microcrystal obtained at same condition as (a), but with 1.5 mg/mL macrocycle **1** concentration. (d) Size distribution calculated based on microcrystal in (c). Red line in (c) and (d) is the normal distribution of microcrystals.

Next we studied the influence of substrates on the fabrication of polydiacetylene microcrystals by spin-coating 1.0 mg/mL macrocycle solution at a rate of 1000 rpm for 90s on glass and quartz substrates. Figure **2.20** gives SEM images of PDA microcrystals generated on glass and quartz slides, similar 1D structures were seen on both substrates. Compared with microcrystals formed on silica wafer, obvious differences in morphology were not observed, this suggests that substrates made minor influence on microcrystal fabrication.

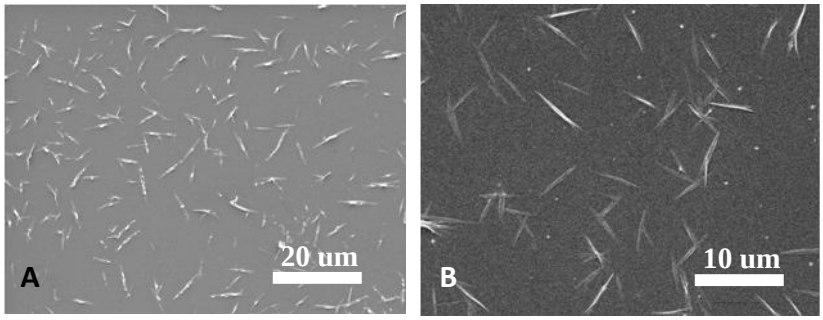

Figure 2.20. (a) SEM image of polydiacetylene microcrystal generated by spin coating 1.0 mg/mL macrocycle **1** solution on glass at a spin-rate of 1000 rpm for 90 s, the spin coated sample was heated at 190 ^{o}C for 3 h to induce the polymerization. (b) PDA microcrystals generated on quartz slide.

2.6.2 Characterization of Polydiacetylene Microcrystals

To monitor the transformation of monomer to polydiacetylene in the microcrystals, we turned to the Raman spectroscopy. Microcrystals generated by spin-coating 1.0 mg/mL macrocycle solution at spin rate of 1000 rpm for 90s on silica wafer were subjected to Raman spectroscopy before and after thermal treatment (Figure **2.21**). Upon heating, the C≡C bond absorption of macrocycle **1** microcrystal at ~2266 cm^{-1} was disappeared. Two new bands were observed at ~1506 and ~2107 cm^{-1}, which corresponding to characteristic carbon double bond and triple bond absorption of polydiacetylene. This suggests that the diacetylene monomer was converted into polydiacetylene during the heating process.

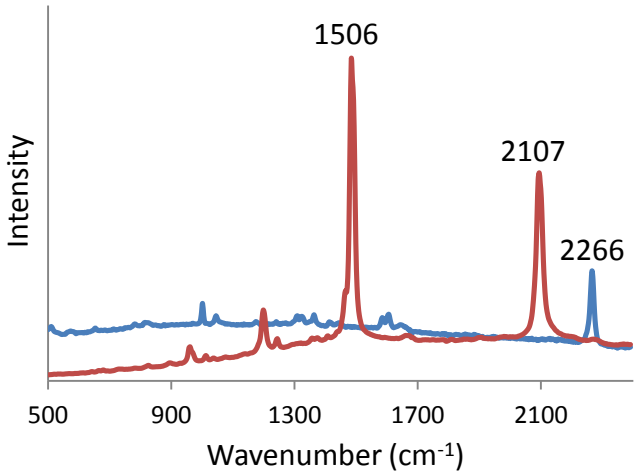

Figure 2.21. Raman spectra (excitation at 632 nm) of macrocycle **1** microcrystal (blue) and thermal treated macrocycle **1** microcrystal (red).

2.7 Study of the Incorporation of Guest Molecules into PDA

Polydiacetylenes (PDA), which classified as conjugated polymers, have attracted attention not only due to their potential sensor applications; but also because of their optical and electronic properties, which originate from the delocalized π electrons along their backbones. These electronic properties give PDAs potential application in devices, such as light emitting diodes (LED) and OFETs. Since most of PDA crystals are nearly insulators and give low conductivity around 10^{-12} S/cm, chemical dopants, such as iodine[34], hydrazine[35], AsF_5[36], $NOPF_6$[37, 38], $FeCl_3$ and $SbCl_5$[39] were investigated to improve the conductivity of PDAs. Herein, we also examined the doping of iodine into PDA crystals and use micro organic field-effect transistor (micro-OFET) devices to characterize the conductivity of iodine treated PDAs in collaboration with Dr. Andrew Greytak and graduate student Paveen Paudel. A single preliminary study showed a roughly linear *I-V* curve obtained for iodine treated PDA crystals. This indicates essentially ohmic conduction, and the conductivity was estimated around 10^{-5}-10^{-4} S/cm.

Such conductivity studies require multiple repeats to establish that the *I-V* curve is reproducible. However, our early study this suggests that iodine doping could improve the conductivity of PDA crystals. Further characterizations are underway to investigate the interaction between PDA crystal and the iodine dopants.

2.7.1 I_2 Treatment of PDA Crystals

Iodine doped PDA crystals (PDA•I_2 complex) were obtained through vapor loading at room temperature. After consultation with Dr. Greytak, I assembled a special iodine loading chamber to prevent surface absorption. The iodine doping system was shown in Figure **2.22**, in this system, flowmeter **1** was used to control the N_2 gas (*F1*), flowmeter **2** was used to control the flow of N_2 gas went into the iodine chamber, then iodine vapor was carried out of the chamber by N_2 (*F2*),. The two flows mixed together in the loading chamber and the iodine partial press PI_2 in the lading chamber was controlled by equation $PI_2 = PI_2^* \times F1/(F1 + F2)$, where PI_2^* was the vapor press of iodine at room temperature. In the iodine doping experiment, we controlled PI_2 to $0.5\ PI_2^*$. The degree of doping was measured by TGA, the iodine doping reached saturation while keeping PDA crystals in loading chamber for two days. The iodine to PDA monomer unit ratio was calculated as 1:14 I_2 to PDA.

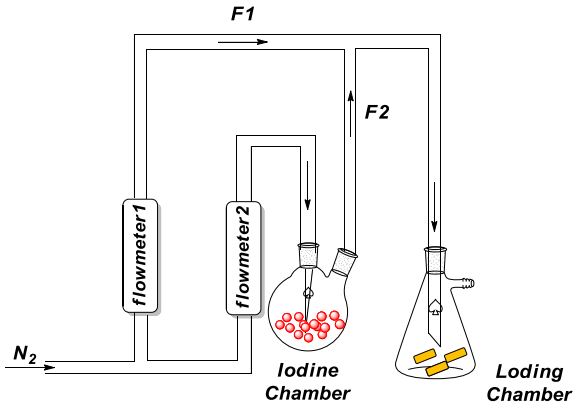

Figure 2.22. Schematic representation of system designed for iodine doping.

2.7.2 Characterization of I_2 Treated PDA

XPS was first used to examine the iodine saturated PDA crystals, and the measurements were conducted by using Kratos AXIS Ultra DLD XPS system, which was equipped with a monochromatic Al Kα source. The monochromatic Al Kα source was operated at 15 keV and 120 W, and the pass energy was fixed at 40 eV for the detailed scans. The binding energy was calibrated using an Ag foil with $Ag3d_{5/2}$ set at 368.21 ± 0.025 eV for the monochromatic Al X-ray source.

Due to the surface charging, a charge neutralizer (CN) was used to do the compensation, and led to the shift of XPS peaks to the lower binding energy area. Therefore the XPS spectra needed to be calibrated before making any comparison. While rigorously there are ten chemically distinct carbon environments in polydiacetylene, in practice XPS may not distinguish between the eight types of hydrocarbons, six from phenyl ring and the rest from the polydiacetylene multiple bonds[40]. Hence, the XPS peaks were corrected according to the core level binding energy (BE) of hydrocarbons which generally accepted at 284.5 eV.

Survey scan for empty PDA and PDA•I_2 complex are shown in Figure **2.23a** and **2.23b** respectively. The XPS spectrum of PDA composed of three peaks that are assigned to C 1s around 285 eV, N 1s around 400 eV and O 1s around 532 eV. In comparison, two new peaks located at ~618 eV and ~630 eV are observed in the spectrum of PDA•I_2 complex, these two peaks are respectively singed to the iodine $3d_{5/2}$ and $3d_{3/2}$ photoemission with a constant shift of 11.5 eV, and which indicated iodine had been incorporated into the PDA crystal.

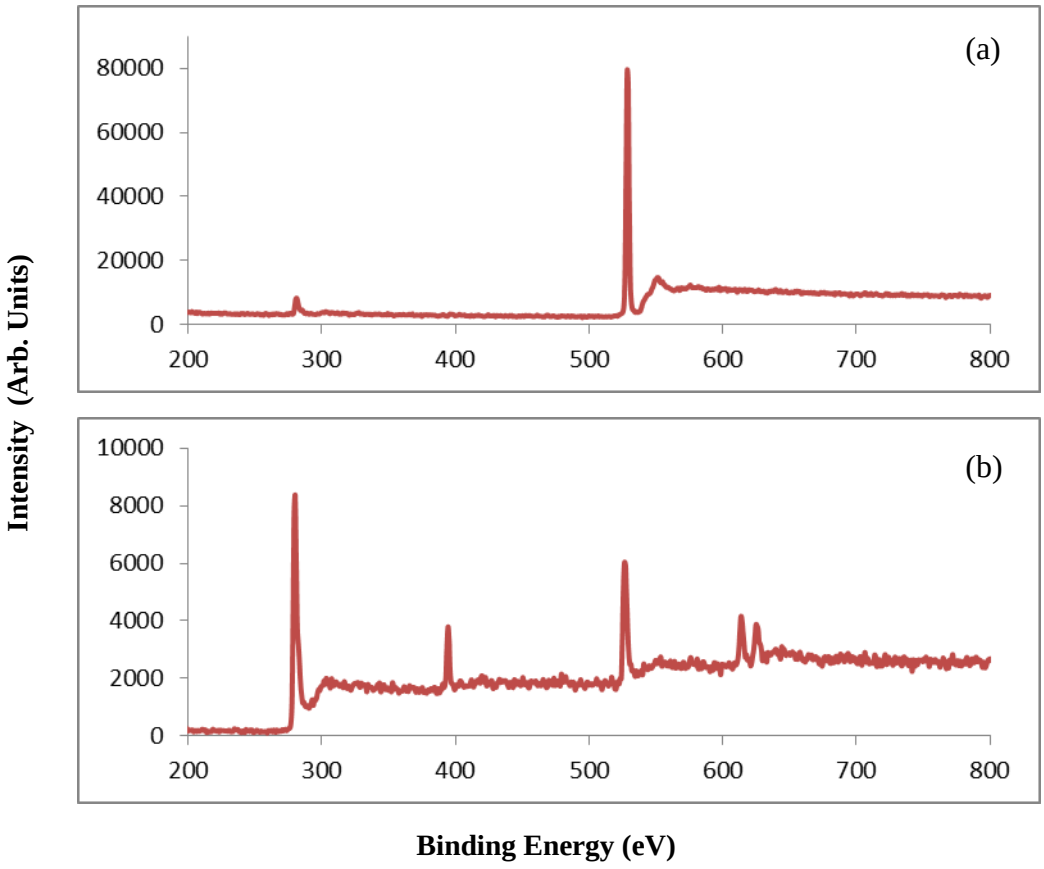

Figure 2.23. Comparison of XPS survey scans: (a) PDA crystal; (b) PDA crystal doped with I_2.

Table **2.1** is the deconvolution results of C 1s, N 1s, O 1s and I $3d_{5/2}$ XPS spectra of empty PDA and PDA•I_2 complex. As shown in Table 1, the C 1s spectrum of PDA could be resolved into three peaks at different binding energies, the peak at 284.5 eV attributed to hydrocarbons including both phenyl ring and polydiacetylene multiple bond carbons. The peak at 286.4 eV attributed to the -CH_2 carbon in the macrocycle and the 288.7 eV peak assigned to the photoemission of the carbonyl carbon in the amide groups[41, 42]. According to Table 1, binding energy of N 1s and O 1s in PDA is 399.9 and 532.3 eV[41, 42]. After doped with iodine, I $3d_{5/2}$ and $3d_{3/2}$ peaks are observed in the spectra, I $3d_{5/2}$ could be deconvoluted into two peaks at 618.3 and 620.4 eV, which indicted the existence of two types of iodine in the iodine doped PDA, and these two peaks are attributed to triiodide I_3^- and pentaiodide I_5^- respectively[41-44]. Besides that, both C=O and CH_2 C 1s peaks shifted to 287.6 and 285.5 eV after iodine incorporated into PDA, and a new O 1s peak also found at 531.1 eV. The chemical shift of C=O C 1s and O 1s photoemission to the lower binding energy area suggests that the carbonyl in PDA might associate with the polyiodide anions.

TABLE 2.1: Core Level Binding Energy (BE) Position for PDA crystal before and after Iodine Doping

Polydiacetylene (PDA)			**I_2 doped Polydiacetylene (PDA)**		
Peak	Assignment	BE (eV)	Peak	Assignment	BE (eV)
C 1s	Hydrocarbons	284.5	C 1s	Hydrocarbons	284.5
	CH_2	286.4		CH_2	285.5
	CONH	288.7		CONH	287.6
N 1s	NH	399.9	N 1s	NH	399.4
O 1s	C=O	532.3	O 1s	$C=O^1$	532.4
				$C=O^2$	531.1
			I $3d_{5/2}$	I_3^-	618.3
				I_5^-	620.4

Figure **2.24** gives the Raman spectra of PDA and PDA•I_2 complex. The Raman spectrum of PDA consists of four main peaks. Peaks located at ~1506 and ~2107 cm^{-1} corresponding to the stretch of double and triple bonds in PDA, Peak at ~941 cm^{-1} assigned to the -CH deformation of aromatic ring and peak at ~1200 cm^{-1} might come from the C-N stretch of the amide groups. After doped with iodine, -CH deformation and C-N stretch peaks shifted to the high energy area, the detail of the shift is shown in the inset diagram of Figure **2.24**, which further indicates that there must be some interactions between the polyiodide anions and the amide carbonyl.

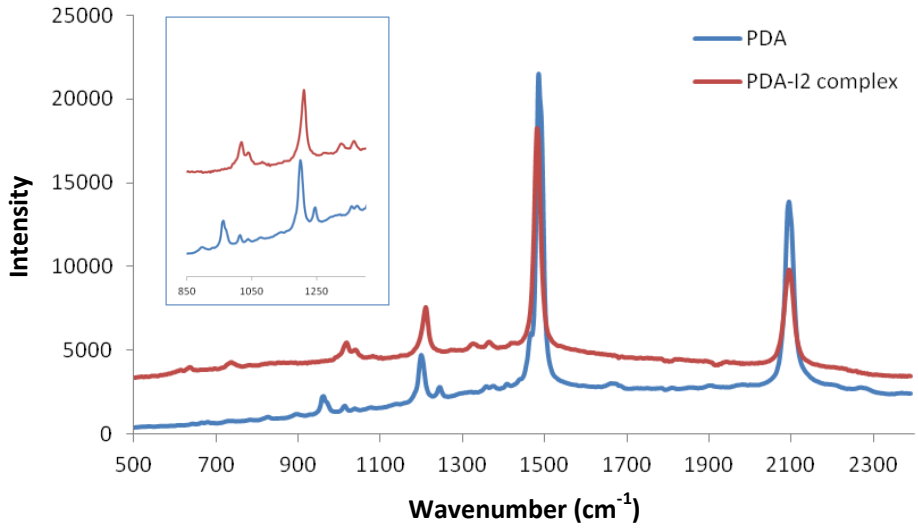

Figure 2.24. Comparison of Raman spectra of PDA before and after doped with iodine

2.8 Summary

We have successfully scaled the synthesis of diacetylene macrocycle **1**. As reported previously, this macrocycle can self-assemble into columnar structure. This chapter has demonstrated that we can obtain three different crystalline forms under different crystallization conditions. Most importantly, we have demonstrated for the first time that thermal treatment of crystal **I** gave a single crystal to single crystal polymerization and have obtained good quality crystals of the resultant PDA. We also investigated the fabrication of polydiacetylene microcrystals by spin-coating technique. We investigated the doping of PDA crystal with iodine vapor under room temperature. Preliminary conductivity tests were carried out in collaboration with Dr. Greytak's group and indicated that iodine doping can improve the conductivity of PDAs. Furthermore, the interaction between iodine dopant and PDA crystals was studied by XPS, Raman and other techniques. Current effort is focused on repeating these conductivity measurements.

2.9 Experiment details

Materials and instruments: All chemicals were purchased from either Sigma-Aldrich or VWR and used without further purification. ^{1}H-NMR was recorded on Varian Mercury/VX 300 and 400 NMR spectrometer. The solid-state NMR experiments were collected on a Varian Inova 500 equipped with Doty XC-4mm magic angle spinning (MAS) probe. Raman spectra were recorded with a J Y Horiba LabRam System using a 632 nm excitation laser. Solution UV-vis data were obtained using a Perkin Elmer Lambda 35 UV/vis scanning spectrophotometer. The solid-state UV-visible spectroscopic data was collected using a Perkin Elmer Lambda 35 UV-Visible scanning spectrophotometer equipped with an integrating sphere. X-ray diffraction data were collected on Bruker SMART APEX diffractometer. PXRD experiments were performed on Rigaku D/Max 2100 Powder X-ray Diffractometer (Cu K radiation). PXRD measurements were taken using a zero background slide onto which the sample was gently pressed. The data was collected at increments of 0.05 degrees and an exposure time of 5 s/step in the angular range of 2-50 degree 2-Theta at ambient temperature. XPS measurements were conducted by using Kratos AXIS Ultra DLD XPS system which equipped with a monochromatic Al Kα source. The monochromatic Al Kα source was operated at 15 keV and 120 W and the pass energy was fixed at 40 eV for the detailed scans.

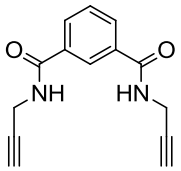

Synthesis of diamide intermediate. Isophthaloyl Chloride (0.5 g, 2.46 mmol) and Et_3N (1.0 mL) were stirred in CH_2Cl_2 (40 mL) and propargylamine (0.35 mL, 0.143 mol) was added. The reaction was stirred at room temperature for three days. Upon completion, the mixture was diluted with 100 mL 1 N HCl and extracted with CH_2Cl_2 (2 × 100 mL). The combined organic extracts were dried over $MgSO_4$ and solvents were removed in *vacuo* to give a light grey solid. Purification by column chromatography (silica gel, CH_2Cl_2/MeOH 97:3) gave the desired diamide (0.4423 g, 0.0018 mol, 75%) as a white solid. Data: ^{1}H-NMR (300 MHz, DMSO-d_6) δ 9.04 (t, *J* = 5.4 Hz, 2 H), 8.32 (s, 1 H), 7.98 (d, *J* = 7.8 Hz, 2 H), 7.57 (t, *J* = 7.8 Hz, 1 H), 4.06 (dd, *J* = 2.4, 5.6 Hz, 4 H), 3.14 (s, 2 H).

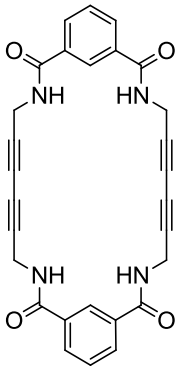

1

Synthesis of macrocycle **1**: The diamide intermediate (0.5 g, 2.08 mmol) was stirred in 50 mL reagent grade DMSO and 1.7 mL pyridine was added. To this stirred solution was added $Cu(OAc)_2$•H_2O (0.25g, 2.08 mmol). The reaction was stirred at r.t. in

the dark for six days. Upon completion as indicated from disappearance of S.M. on TLC (CH_2Cl_2/MeOH, 90:10), the reaction was diluted with 1 N HCl (100 mL). The resulting precipitate was filtered and washed with 1 N HCl (2 × 100 mL), H_2O (2 × 100 mL) and CH_2Cl_2 (3 × 100 mL). The grey solid was dried *in vacuo* in the dark. The crude product was purified by column chromatography (silica gel, CH_2Cl_2/MeOH 90:10). The finally product was light yellow solid (75 mg, 15%). Data: ^{1}H-NMR (400 MHz, DMSO-d_6) δ 9.14 (t, J = 4.8 Hz, 4 H), 8.31 (s, 2 H), 7.92 (d, J = 7.6 Hz, 4 H), 7.56 (t, J = 7.6 Hz, 2 H), 4.16 (d, J = 4.8 Hz, 8 H).

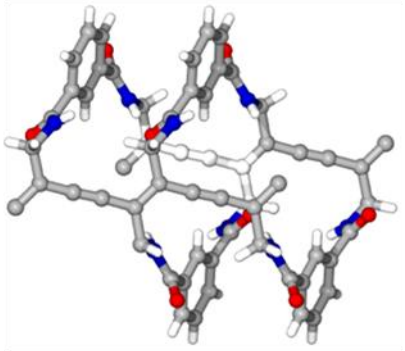

Synthesis of PDA. The crystal **I** of macrocycle **1** (10 mg) were placed in a vial and heated in a sand bath at 190 ℃ for 12 hours under the flow of N_2. The heated material turned dark purple/brown and was insoluble in DMSO and in most organic solvent. No monomer was detected by solid state ^{1}H-^{13}C COSY (HETCOR), which indicated efficient conversion to polymeric material. Data: ^{13}C-NMR δ 165 (broad), 130 (broad), 106, 101, 44. ^{1}H-NMR δ 9.8 (broad), 7.2 (broad). Raman: 1506, 2107 cm^{-1}.

2.9.1 X-ray Crystal Structure Data

X-Ray Structure Determination, $C_{28}H_{20}N_4O_4 \cdot 2(H_2O)$ (crystal I)

X-ray intensity data from a red needle crystal were measured at 150(2) K on a Bruker SMART APEX diffractometer (Mo Kα radiation, λ = 0.71073 Å).1 Raw area detector data frame processing was performed with the SAINT+ and SADABS programs.[1] Final unit cell parameters were determined by least-squares refinement of 6132 reflections from the data set. Direct methods structure solution, difference Fourier calculations and full-matrix least-squares refinement against F2 were performed with SHELXTL.[2]

The compound crystallizes in the space group $P2_1/c$ as determined by the pattern of systematic absences in the intensity data. The asymmetric unit consists of half of one $C_{28}H_{20}N_4O_4$ molecule located on a crystallographic inversion center, and one water molecule. Location and refinement of the water hydrogen atoms was problematic. Three electron density peaks near the water oxygen atom were clearly present in difference maps, in plausible positions for hydrogen atoms. Trial refinements indicated partial occupancy of two of the hydrogen positions, consistent with a water molecule disordered over two orientations. This was determined by fixing a reasonable isotropic displacement parameter value of Uiso = 0.05 $Å^2$ for all three peaks and refining their site occupancy factors. Two of the three peaks refined to partial occupancy (H3A and H3B), while the third remained at full occupancy (H3AB). For subsequent refinement cycles, the occupancies were fixed near the refined values (H3A = 0.60; H3B = 0.40) and a common Uiso value refined for all three hydrogen atoms. O-H distances were restrained to be similar (three restraints). All non-hydrogen atoms were refined with anisotropic

displacement parameters. Hydrogen atoms bonded to carbon were located indifference maps before being placed in geometrically idealized positions and included as riding atoms. The nitrogen-bound hydrogen atoms H1 and H2 were located in difference maps and refined freely.

(1) SMART Version 5.630, SAINT+ Version 6.45 and SADABS Version 2.10. Bruker Analytical X-ray Systems, Inc., Madison, Wisconsin, USA, 2003.

(2) Sheldrick, G. M. SHELXTL Version 6.14; Bruker Analytical X-ray Systems, Inc., Madison, Wisconsin, USA, 2000.

Crystal data and structure refinement for lss131s.

Identification code	lss131s
Empirical formula	C_{28} H_{24} N_4 O_6
Formula weight	512.51
Temperature/K	150(2) K
Crystal system	Monoclinic
Space group	P21/c
a/Å	4.9860(2)
b/Å	14.6944(7)
c/Å	16.8680(8)
α/°	90
β/°	96.9050(10)
γ/°	90
Volume/Å^3	1226.89(10)
Z	2
ρ_{calc}mg/mm^3	1.387

m/mm^{-1}	0.099
F(000)	536
Crystal size/mm^3	0.66 x 0.10 x 0.08 mm^3
2Θ range for data collection	1.84 to 26.42 °.
Index ranges	6<=h<=6, -18<=k<=18, -21<=l<=21
Reflections collected	17823
Independent reflections	2522 [R(int) = 0.0343]
Data/restraints/parameters	2522/3/190
Goodness-of-fit on F^2	1.035
Final R indexes [I>=2σ (I)]	R_1 = 0.0418, wR_2 = 0.1047
Final R indexes [all data]	R_1 = 0.0488, wR_2 = 0.1102
Largest diff. peak/hole / e $Å^{-3}$	0.297 and -0.204 e.$Å^{-3}$

X-Ray Structure Determination, $C_{28}H_{20}N_4O_4$ (CH_3OH) (Crystal II)

Intensity data were collected at **150K** on a D8 goniostat equipped with a Bruker APEXII CCD detector at Beamline 11.3.1 at the Advanced Light Source (Lawrence Berkeley National Laboratory) using synchrotron radiation tuned to **λ=0.7749Å**.[1] The data crystal was a small pale blue block of approximate dimensions 0.04 x 0.03 x 0.03 mm^3. For data collection frames were measured for a duration of 1-s at 0.3º intervals of ω with a maximum 2θ value of ~60º. The data frames were collected using the program APEX2 and processed using the program SAINT within APEX2.[2] The data were corrected for absorption and beam corrections based on the multi-scan technique as

implemented in SADABS.[2] Direct methods structure solution, difference Fourier calculations and full-matrix least-squares refinement against F^2 were performed with SHELXS/L[3] as implemented in OLEX2.[4]

The compound crystallizes in the triclinic system. The space group P-1 (No. 2) was determined by obtaining a reasonable solution and refinement of the disordered structure. The asymmetric unit consists of half of one disordered $C_{28}H_{20}N_4O_4$ cycle situated about a crystallographic inversion center and a fractionally populated, disordered solvent region which was modeled as methanol. The disorder of the cycle is caused by the presence of two opposite conformations of the -C(O)NH- group (C8, O2, N2), and also affects the phenyl ring atoms C2-C7 and atoms C12-C14 of the attached -CH_2CC- grouping. The two conformations were refined as equally populated, with the aid of nine distance restraints. They were numbered identically except for suffixes A or B. The methanol guest is disordered over two unique sites with refined occupancies of O3S/O4S = 0.279(7)/0.221(7). The total methanol site occupancy was constrained to sum to 0.5. This population constraint is necessary because of the close steric proximity of the 50%-occupied carbonyl oxygen O2B of the cycle (O2B---O3S/O4S < 1.8 Å). The two unique methanol sites are located near an inversion center, and thus four sites with total population 1.0 are generated per cycle. Atoms affected by disorder were refined isotropically. Only the non-disordered atoms O1, N1, C1, C9-C11 were refined with anisotropic displacement parameters. Hydrogen atoms were placed in geometrically idealized positions and included as riding atoms. The high R-values are because of the extensive whole-molecule and solvent disorder. The disorder is not imposed by the

inversion symmetry of the centric space group P-1 (No. 2), as the same conformational disorder was also observed in trial refinements in space group P1 (No. 1).

(1) Crystallographic data were collected through the SCrALS (Service Crystallography at Advanced Light Source) program at the Small-Crystal Crystallography Beamline 11.3.1 at the Advanced Light Source (ALS), Lawrence Berkeley National Laboratory. The ALS is supported by the U.S. Department of Energy, Office of Energy Sciences Materials Sciences Division, under contract DE-AC02-05CH11231.

(2) APEX2 v2012.2.0 and SAINT v7.68A data collection and data processing programs, respectively. Bruker Analytical X-ray Instruments, Inc., Madison, WI; SADABS v2008/1 semi-empirical absorption and beam correction program. G.M. Sheldrick, University of Göttingen, Germany.

(3) Sheldrick, G.M. *Acta Cryst*. **2008**, A64, 112-122.

(4) Dolomanov, O. V., Bourhis, L. J., Gildea, R. J., Howard J. A. K. and Puschmann, H. OLEX2: a complete structure solution, refinement and analysis program. *J. Appl. Cryst.* **2009**, *42*, 339-341.

Crystal data and structure refinement for usca023b

Identification code	usca023b
Empirical formula	$C_{29}H_{24}N_4O_5$
Formula weight	508.52
Temperature/K	150(2)
Crystal system	triclinic
Space group	P-1

a/Å	4.5301(10)
b/Å	11.579(3)
c/Å	12.321(3)
α/°	111.787(3)
β/°	99.823(3)
γ/°	97.184(3)
Volume/$Å^3$	578.7(2)
Z	1
$\rho_{calc}mg/mm^3$	1.459
m/mm^{-1}	0.102
F(000)	266.0
Crystal size/mm^3	0.04 × 0.03 × 0.03
2Θ range for data collection	6.78 to 56.56 °
Index ranges	$-6 \leq h \leq 6$, $-15 \leq k \leq 15$, $-16 \leq l \leq 16$
Reflections collected	7750
Independent reflections	2841[R(int) = 0.0357]
Data/restraints/parameters	2841/9/134
Goodness-of-fit on F^2	1.088
Final R indexes [I>=2σ (I)]	R_1 = 0.0989, wR_2 = 0.2670
Final R indexes [all data]	R_1 = 0.1339, wR_2 = 0.2975
Largest diff. peak/hole / e $Å^{-3}$	0.87/-0.56

X-Ray Structure Determination, $C_{28}H_{20}N_4O_4 \cdot 4(H_2O)$ (Crystal III)

X-ray intensity data from a colorless needle crystal were measured at 295(2) K using a Bruker SMART APEX diffractometer (Mo Ka radiation, l = 0.71073 Å).[1] All crystals examined were found to be twinned. The data crystal was a two-component non-merohedral twin. Identification of the twinning, derivation of the twin law and creation of input files for data reduction were performed using the Bruker GEMINI software program.[1] The twin domains are related by a 180 °rotation around the real-space direction [011]. The twin law is, by rows, [-1 -0.815 -0.815 / 0 -0.066 0.933 / 0 1.067 0.066]. The major twin fraction refined to 0.540(4). The raw area detector data frames were reduced and corrected for absorption effects with the SAINT+ and TWINABS programs.[1] The reported R(int) value was taken from the TWINABS output. Final unit cell parameters were determined by least-squares refinement of 3169 reflections from the data set. Direct methods structure solution, difference Fourier calculations and full-matrix least-squares refinement against F^2 were performed with SHELXS/L[2] as implemented in OLEX2.[3]

The compound crystallizes in the triclinic system. The space group P-1 (No. 2) was confirmed by the successful solution and refinement of the structure. The asymmetric unit consists of half of one $C_{28}H_{20}N_4O_4$ cycle which is situated about a crystallographic inversion center, and two independent water molecules. Non-hydrogen atoms were refined with anisotropic displacement parameters. Hydrogen atoms bonded to carbon were placed in geometrically idealized positions and included as riding atoms. Hydrogen atoms bonded to nitrogen and oxygen were located in difference maps and refined isotropically. The water hydrogens were restrained to have similar O-H distances and were assigned a common displacement parameter.

(1) SMART Version 5.630, GEMINI, SAINT+ Version 6.45 and TWINABS. Bruker Analytical X-ray Systems, Inc., Madison, Wisconsin, USA, 2003.

(2) Sheldrick, G.M. *Acta Cryst*. **2008**, *A64*, 112-122.

(3) Dolomanov, O. V., Bourhis, L. J., Gildea, R. J., Howard J. A. K. and Puschmann, H. OLEX2: a complete structure solution, refinement and analysis program. *J. Appl. Cryst.* **2009**, *42*, 339-341.

Crystal data and structure refinement for wx171s2

Identification code	wx171s2
Empirical formula	$C_{28}H_{28}N_4O_8$
Formula weight	548.54
Temperature/K	295(2)
Crystal system	triclinic
Space group	P-1
a/Å	8.9148(5)
b/Å	9.4752(5)
c/Å	9.8948(5)
α/°	110.584(1)
β/°	108.502(1)
γ/°	104.815(1)
Volume/Å^3	675.53(6)
Z	1
ρ_{calc}mg/mm^3	1.348
m/mm^{-1}	0.100

F(000)	288.0
Crystal size/mm^3	0.56 × 0.08 × 0.04
2Θ range for data collection	4.92 to 48.24 °
Index ranges	$-10 \leq h \leq 9$, $-10 \leq k \leq 10$, $0 \leq l \leq 11$
Reflections collected	2200
Independent reflections	2200[R(int) = 0.0443]
Data/restraints/parameters	2200/6/203
Goodness-of-fit on F^2	0.893
Final R indexes [I>=2σ (I)]	R_1 = 0.0406, wR_2 = 0.0803
Final R indexes [all data]	R_1 = 0.0737, wR_2 = 0.0920
Largest diff. peak/hole / e $Å^{-3}$	0.17/-0.16

X-Ray Structure Determination, $C_{28}H_{20}N_4O_4$ (PDA)

X-ray intensity data from a dark red needle crystal were collected at 100(2) K using a Bruker SMART APEX diffractometer (Mo Ka radiation, l = 0.71073 Å).[1] The raw area detector data frames were reduced with the the SAINT+ and SADABS programs.[1] Final unit cell parameters were determined by least-squares refinement of 1196 reflections from the data set. Direct methods structure solution, difference Fourier calculations and full-matrix least-squares refinement against F^2 were performed with SHELXS/L^2 within OLEX2.[3]

The compound crystallizes in the monoclinic space group $P2_1/c$ as determined by the pattern of systematic absences in the intensity data. The asymmetric unit consists of half of one polymeric formula unit, which is situated about a crystallographic inversion center. All non-hydrogen atoms were refined with anisotropic displacement parameters.

Hydrogen atoms bonded to carbon were located in difference maps before being placed in geometrically idealized positions and included as riding atoms. Hydrogen atoms bonded to nitrogen were located in difference maps and refined freely.

(1) SMART Version 5.630, SAINT+ Version 6.45 and SADABS Version 2.10. Bruker Analytical X-ray Systems, Inc., Madison, Wisconsin, USA, 2003.

(2) Sheldrick, G.M. *Acta Cryst*. **2008**, A64, 112-122.

(3) Dolomanov, O. V., Bourhis, L. J., Gildea, R. J., Howard J. A. K. and Puschmann, H. OLEX2: a complete structure solution, refinement and analysis program. *J. Appl. Cryst.* **2009**, *42*, 339-341.

Crystal data and structure refinement for wwx228a

Identification code	wwx228a
Empirical formula	$C_{28}H_{20}N_4O_4$
Formula weight	476.48
Temperature/K	100(2)
Crystal system	monoclinic
Space group	$P2_1/c$
a/Å	4.895(3)
b/Å	14.586(8)
c/Å	16.285(9)

α/°	90.00
β/°	104.125(11)
γ/°	90.00
Volume/Å^3	1127.7(11)
Z	2
ρ_{calc}mg/mm^3	1.403
μ/mm^{-1}	0.096
F(000)	496.0
Crystal size/mm^3	0.56 × 0.04 × 0.03
2Θ range for data collection	3.8 to 48.5 °
Index ranges	$-5 \leq h \leq 5$, $-16 \leq k \leq 16$, $-18 \leq l \leq 18$
Reflections collected	12582
Independent reflections	1821[R(int) = 0.1021]
Data/restraints/parameters	1821/0/171
Goodness-of-fit on F^2	1.072
Final R indexes [I>=2σ (I)]	R_1 = 0.0599, wR_2 = 0.1354

Final R indexes [all data] $R_1 = 0.0831$, $wR_2 = 0.1460$

Largest diff. peak/hole / e $Å^{-3}$ 0.35/-0.22

X-Ray Structure Determination for Single Crystal to Single Crystal Transformation

$C_{28}H_{20}N_4O_4 \cdot 2(H_2O)$ and $C_{28}H_{20}N_4O_4$ (PDA monomer hydrate and polymer)

The single crystal-to-single crystal nature of the transformation was verified by performing the X-ray intensity data collections before and after the thermal polymerization process using the same crystal. For data collection of the unheated sample, a dark red needle crystal of dimensions 0.52 x 0.05 x 0.04 mm^3 was selected. After data collection and structure determination, the data crystal was removed from the diffractometer, placed on a glass slide and its position on the slide noted. The data crystal was then subjected to the thermal polymerization process. When this was completed, the glass slide and data crystal was returned to the X-ray lab and examined. The position of the crystal on the glass slide as well as the crystal shape and color appeared unchanged. Another data collection was performed on the heated crystal. A different unit cell with a smaller volume was indexed (see crystal data). Analysis of the diffraction peak profiles showed the sample crystallinity was retained with minimal degradation. Peak shapes were broader and high-angle reflections were weaker in intensity, though still acceptable. Details of each structure solution are given below. The single crystal-to-single crystal transformation occurs without a change in space group symmetry ($P2_1/c$ for both forms) or unit cell volume beyond a 9% contraction, which is primarily due to loss of the interstitial water molecule guests and the creation of hydrogen bonds between polymeric columns. The structural transition is therefore not accompanied by twinning. Both X-ray

intensity datasets were collected at 100(2) K using a Bruker SMART APEX diffractometer (Mo Ka radiation, l = 0.71073 Å).[1] The raw area detector data frames were reduced with the the SAINT+ and SADABS programs.[1] Final unit cell parameters were determined by least-squares refinement of large sets of strong reflections from each data set. Direct methods structure solution, difference Fourier calculations and full-matrix least-squares refinement against F^2 were performed with SHELXS/L[2] within OLEX2.[3]

$C_{28}H_{20}N_4O_4 \cdot 2(H_2O)$ (PDA hydrate monomer): The compound crystallizes in the space group $P2_1/c$ as determined uniquely by the pattern of systematic absences in the intensity data. The asymmetric unit consists of half of one cycle and two primary peaks corresponding to interstitial guest species. The cycle and the two guest solvent peaks are situated about a crystallographic inversion center. The interstitial peaks were modeled as two fractionally populated oxygen atoms of water molecules. The two peaks had different magnitudes in the Fourier difference map, and therefore a model using methanol was attempted. This resulted in similar R-factors but an unreasonably short C-O distance of *ca*. 1.3 Å. The disordered water molecule model was therefore retained. Some methanol may be present, but its identification is uncertain because of the disorder. All non-hydrogen atoms were refined with anisotropic displacement parameters. The U_{ij} values for the water molecule oxygen atoms were held equal, and the total site population constrained to sum to unity. Hydrogen atoms bonded to carbon were placed in geometrically idealized positions and included as riding atoms. Hydrogen atoms bonded to nitrogen were located in difference maps and refined freely. The water hydrogens could not be located and were not calculated. The largest residual electron density peak of 0.51 $e^-/Å^3$ in the final difference map is located 0.77 Å from O3, in the disordered guest molecule volume.

$C_{28}H_{20}N_4O_4$ (polymer): The compound crystallizes in the monoclinic space group $P2_1/c$ as determined uniquely by the pattern of systematic absences in the intensity data. The asymmetric unit consists of half of one polymeric formula unit, which is situated about a crystallographic inversion center. All non-hydrogen atoms were refined with anisotropic displacement parameters. Hydrogen atoms bonded to carbon were located in difference maps before being placed in geometrically idealized positions and included as riding atoms. Hydrogen atoms bonded to nitrogen were located in difference maps and refined freely.

Notes: The largest contraction of the unit cell as a result of the transformation is along the *c* axis, because of the formation of an inter-columnar NH---O hydrogen bond along that direction.

(1) SMART Version 5.630, SAINT+ Version 6.45 and SADABS Version 2.10. Bruker Analytical X-ray Systems, Inc., Madison, Wisconsin, USA, 2003.

(2) Sheldrick, G.M. *Acta Cryst*. **2008**, A64, 112-122.

(3) Dolomanov, O. V., Bourhis, L. J., Gildea, R. J., Howard J. A. K. and Puschmann, H. OLEX2: a complete structure solution, refinement and analysis program. *J. Appl. Cryst.* **2009**, *42*, 339-341.

2.10 Reference

(1) Moerner, W. E.; Silence, S. M. *Chem Rev* **1994**, *94*, 127.

(2) Bundgaard, E.; Krebs, F. C. *Sol Energ Mat Sol C* **2007**, *91*, 954.

(3) Thomas, S. W.; Joly, G. D.; Swager, T. M. *Chem Rev* **2007**, *107*, 1339.

(4) Xu, Y. W.; Smith, M. D.; Geer, M. F.; Pellechia, P. J.; Brown, J. C.; Wibowo, A. C.; Shimizu, L. S. *J Am Chem Soc* **2010**, *132*, 5334.

(5) Wegner, G. A. *Naturforsch. Teil B* **1969**, *24*.

(6) Andrew, T. L.; Swager, T. M. *J Polym Sci Pol Phys* **2011**, *49*, 476.

(7) Yang, S. J.; Kertesz, M. *J Phys Chem A* **2006**, *110*, 9771.

(8) Okada, S.; Peng, S.; Spevak, W.; Charych, D. *Accounts Chem Res* **1998**, *31*, 229.

(9) Charych, D. H. *Science* **1993**, *261*, 1375.

(10) Yoon, J.; Chae, S. K.; Kim, J. M. *J Am Chem Soc* **2007**, *129*, 3038.

(11) Lee, J.; Yarimaga, O.; Lee, C. H.; Choi, Y. K.; Kim, J. M. *Adv Funct Mater* **2011**, *21*, 1032.

(12) Pindzola, B. A.; Nguyen, A. T.; Reppy, M. A. *Chem Commun* **2006**, 906.

(13) Chang, Y. L.; West, M. A.; Fowler, F. W.; Lauher, J. W. *J Am Chem Soc* **1993**, *115*, 5991.

(14) Coe, S.; Kane, J. J.; Nguyen, T. L.; Toledo, L. M.; Wininger, E.; Fowler, F. W.; Lauher, J. W. *J Am Chem Soc* **1997**, *119*, 86.

(15) Nguyen, T. L.; Fowler, F. W.; Lauher, J. W. *J Am Chem Soc* **2001**, *123*, 11057.

(16) Curtis, S. M.; Le, N.; Nguyen, T.; Xi, O. Y.; Tran, T.; Fowler, F. W.; Lauher, J. W. *Supramol Chem* **2005**, *17*, 31.

(17) Gravel, E.; Ogier, J.; Arnauld, T.; Mackiewicz, N.; Duconge, F.; Doris, E. *Chem-Eur J* **2012**, *18*, 400.

(18) Kim, I. B.; Dunkhorst, A.; Bunz, U. H. F. *Langmuir* **2005**, *21*, 7985.

(19) Ahn, D. J.; Lee, S.; Kim, J. M. *Adv Funct Mater* **2009**, *19*, 1483.

(20) Nantalaksakul, A.; Krishnamoorthy, K.; Thayumanavan, S. *Macromolecules* **2010**, *43*, 37.

(21) Coakley, K. M.; McGehee, M. D. *Chem Mater* **2004**, *16*, 4533.

(22) Lauher, J. W.; Fowler, F. W.; Goroff, N. S. *Accounts Chem Res* **2008**, *41*, 1215.

(23) Hsu, T. J.; Fowler, F. W.; Lauher, J. W. *J Am Chem Soc* **2012**, *134*, 142.

(24) Socrates, G. *Infrared and Raman characteristic group frequencies : tables and charts*; 3rd ed.; Wiley: Chichester, **2001**.

(25) Xu, R.; Schweizer, W. B.; Frauenrath, H. *Chem-Eur J* **2009**, *15*, 9105.

(26) Yoon, J.; Kim, J. M. *Macromol Chem Phys* **2008**, *209*, 2195.

(27) Lifshitz, Y.; Golan, Y.; Konovalov, O.; Berman, A. *Langmuir* **2009**, *25*, 4469.

(28) Cho, J. T.; Woo, S. M.; Ahn, D. J.; Ahn, K. D.; Lee, H.; Kim, J. M. *Chem Lett* **2003**, *32*, 282.

(29) Jiang, H.; Pan, X. J.; Lei, Z. Y.; Zou, G.; Zhang, Q. J.; Wang, K. Y. *J Mater Chem* **2011**, *21*, 4518.

(30) Cho, S.; Han, G.; Kim, K.; Sung, M. M. *Angew Chem Int Edit* **2011**, *50*, 2742.

(31) Lee, J.; Yarimaga, O.; Lee, C. H.; Choi, Y. K.; Kim, J. M. *Adv Funct Mater* **2011**, *21*, 1032.

(32) Lee, S. B.; Koepsel, R.; Stolz, D. B.; Warriner, H. E.; Russell, A. J. *J Am Chem Soc* **2004**, *126*, 13400.

(33) Yarimaga, O.; Yoon, B.; Ham, D. Y.; Lee, J.; Hara, M.; Choi, Y. K.; Kim, J. M. *J Mater Chem* **2011**, *21*, 18605.

(34) Tabata, H.; Tokoyama, H.; Yamakado, H.; Okuno, T. *J Mater Chem* **2012**, *22*, 115.

(35) Ellis, D. L. Z., M. R.; Bernstein, L. S.; Rubner, M. F *Polymeric Materials Science and Engineering* **1994**, *71*, 2.

(36) Thomas, H. R.; Salaneck, W. R.; Duke, C. B.; Plummer, E. W.; Heeger, A. J.; Macdiarmid, A. G. *Polymer* **1980**, *21*, 1238.

(37) Groenewoud, L. M. H.; Weinbeck, A. E.; Engbers, G. H. M.; Feijen, J. *Synthetic Met* **2002**, *126*, 143.

(38) Li, J.; Rajca, A.; Rajca, S. *Synthetic Met* **2003**, *137*, 1507.

(39) Sakamoto, M.; Wasserman, B.; Dresselhaus, M. S.; Wnek, G. E.; Elman, B. S.; Sandman, D. J. *J Appl Phys* **1986**, *60*, 2788.

(40) Whelan, C. M.; Cecchet, F.; Baxter, R.; Zerbetto, F.; Clarkson, G. J.; Leigh, D. A.; Rudolf, P. *J Phys Chem B* **2002**, *106*, 8739.

(41) Aldissi, M.; Armes, S. P. *Macromolecules* **1992**, *25*, 2963.

(42) Zeng, X. R.; Ko, T. M. *J Polym Sci Pol Phys* **1997**, *35*, 1993.

(43) Hsu, S. L.; Signorelli, A. J.; Pez, G. P.; Baughman, R. H. *J Chem Phys* **1978**, *69*, 106.

(44) Grigorian, L.; Williams, K. A.; Fang, S.; Sumanasekera, G. U.; Loper, A. L.; Dickey, E. C.; Pennycook, S. J.; Eklund, P. C. *Phys Rev Lett* **1998**, *80*, 5560.

BIBLIOGRAPHY

Eisenberg, B. *Accounts Chem Res* **1998**, *31*, 117.

Borgnia, M.; Nielsen, S.; Engel, A.; Agre, P. *Annu Rev Biochem* **1999**, *68*, 425.

Yoshizawa, M.; Klosterman, J. K.; Fujita, M. *Angew Chem Int Edit* **2009**, *48*, 3418.

Sigler, P. B.; Xu, Z. H.; Rye, H. S.; Burston, S. G.; Fenton, W. A.; Horwich, A. L. *Annu Rev Biochem* **1998**, *67*, 581.

Voges, D.; Zwickl, P.; Baumeister, W. *Annu Rev Biochem* **1999**, *68*, 1015.

Vriezema, D. M.; Aragones, M. C.; Elemans, J. A. A. W.; Cornelissen, J. J. L. M.; Rowan, A. E.; Nolte, R. J. M. *Chem Rev* **2005**, *105*, 1445.

Cram, D. J. *Science* **1983**, *219*, 1177.

Cram, D. J. *Nature* **1992**, *356*, 29.

Nelson, J. C.; Saven, J. G.; Moore, J. S.; Wolynes, P. G. *Science* **1997**, *277*, 1793.

Prince, R. B.; Saven, J. G.; Wolynes, P. G.; Moore, J. S. *J Am Chem Soc* **1999**, *121*, 3114.

Prince, R. B.; Barnes, S. A.; Moore, J. S. *J Am Chem Soc* **2000**, *122*, 2758.

Bong, D. T.; Clark, T. D.; Granja, J. R.; Ghadiri, M. R. *Angew Chem Int Edit* **2001**, *40*, 988.

Yamaguchi, T.; Tashiro, S.; Tominaga, M.; Kawano, M.; Ozeki, T.; Fujita, M. *J Am Chem Soc* **2004**, *126*, 10818.

Percec, V.; Heck, J.; Tomazos, D.; Falkenberg, F.; Blackwell, H.; Ungar, G. *J Chem Soc Perk T 1* **1993**, 2799.

Andrew, T. L.; Swager, T. M. *J Polym Sci Pol Phys* **2011**, *49*, 476.

Yang, S. J.; Kertesz, M. *J Phys Chem A* **2006**, *110*, 9771.

Chen, X.; Kang, S.; Kim, M. J.; Kim, J.; Kim, Y. S.; Kim, H.; Chi, B.; Kim, S. J.; Lee, J. Y.; Yoon, J. *Angew Chem Int Edit* **2010**, *49*, 1422.

Tang, C. W. *Appl Phys Lett* **1986**, *48*, 183.

Sariciftci, N. S.; Smilowitz, L.; Heeger, A. J.; Wudl, F. *Science* **1992**, *258*, 1474.

Hoppe, H.; Egbe, D. A. M.; Muhlbacher, D.; Sariciftci, N. S. *J Mater Chem* **2004**, *14*, 3462.

Okada, S.; Peng, S.; Spevak, W.; Charych, D. *Accounts Chem Res* **1998**, *31*, 229.

Charych, D. H. *Science* **1993**, *261*, 1375.

Yoon, J.; Chae, S. K.; Kim, J. M. *J Am Chem Soc* **2007**, *129*, 3038.

Lee, J.; Yarimaga, O.; Lee, C. H.; Choi, Y. K.; Kim, J. M. *Adv Funct Mater* **2011**, *21*, 1032.

Pindzola, B. A.; Nguyen, A. T.; Reppy, M. A. *Chem Commun* **2006**, 906.

Yang, J. S.; Swager, T. M. *J Am Chem Soc* **1998**, *120*, 5321.

Nantalaksakul, A.; Krishnamoorthy, K.; Thayumanavan, S. *Macromolecules* **2010**, *43*, 37.

Coakley, K. M.; McGehee, M. D. *Chem Mater* **2004**, *16*, 4533.

Xu, Y. W.; Smith, M. D.; Geer, M. F.; Pellechia, P. J.; Brown, J. C.; Wibowo, A. C.; Shimizu, L. S. *J Am Chem Soc* **2010**, *132*, 5334.

Zhou, Q.; Carroll, P. J.; Swager, T. M. *J Org Chem* **1994**, *59*, 1294.

Roy, K.; Wibowo, A. C.; Pellechia, P. J.; Ma, S. G.; Geer, M. F.; Shimizu, L. S. *Chem Mater* **2012**, *24*, 4773.

Roy, K.; Wang, C.; Smith, M. D.; Dewal, M. B.; Wibowo, A. C.; Brown, J. C.; Ma, S. G.; Shimizu, L. S. *Chem Commun* **2011**, *47*, 277.

Thallapally, P. K.; McGrail, B. P.; Dalgarno, S. J.; Schaef, H. T.; Tian, J.; Atwood, J. L. *Nat Mater* **2008**, *7*, 146.

Thallapally, P. K.; Dobrzanska, L.; Gingrich, T. R.; Wirsig, T. B.; Barbour, L. J.; Atwood, J. L. *Angew Chem Int Edit* **2006**, *45*, 6506.

Atwood, J. L.; Barbour, L. J.; Jerga, A.; Schottel, B. L. *Science* **2002**, *298*, 1000.

Shetty, A. S.; Zhang, J. S.; Moore, J. S. *J Am Chem Soc* **1996**, *118*, 1019.

Ranganathan, D.; Haridas, V.; Nagaraj, R.; Karle, I. L. *J Org Chem* **2000**, *65*, 4415.

Ranganathan, D.; Haridas, V.; Gilardi, R.; Karle, I. L. *J Am Chem Soc* **1998**, *120*, 10793.

Moerner, W. E.; Silence, S. M. *Chem Rev* **1994**, *94*, 127.

Bundgaard, E.; Krebs, F. C. *Sol Energ Mat Sol C* **2007**, *91*, 954.

Thomas, S. W.; Joly, G. D.; Swager, T. M. *Chem Rev* **2007**, *107*, 1339.

Wegner, G. A. *Naturforsch. Teil B* **1969**, *24*.

Pindzola, B. A.; Nguyen, A. T.; Reppy, M. A. *Chem Commun* **2006**, 906.

Chang, Y. L.; West, M. A.; Fowler, F. W.; Lauher, J. W. *J Am Chem Soc* **1993**, *115*, 5991.

Coe, S.; Kane, J. J.; Nguyen, T. L.; Toledo, L. M.; Wininger, E.; Fowler, F. W.; Lauher, J. W. *J Am Chem Soc* **1997**, *119*, 86.

Nguyen, T. L.; Fowler, F. W.; Lauher, J. W. *J Am Chem Soc* **2001**, *123*, 11057.

Curtis, S. M.; Le, N.; Nguyen, T.; Xi, O. Y.; Tran, T.; Fowler, F. W.; Lauher, J. W. *Supramol Chem* **2005**, *17*, 31.

Gravel, E.; Ogier, J.; Arnauld, T.; Mackiewicz, N.; Duconge, F.; Doris, E. *Chem-Eur J* **2012**, *18*, 400.

Kim, I. B.; Dunkhorst, A.; Bunz, U. H. F. *Langmuir* **2005**, *21*, 7985.

Ahn, D. J.; Lee, S.; Kim, J. M. *Adv Funct Mater* **2009**, *19*, 1483..

Lauher, J. W.; Fowler, F. W.; Goroff, N. S. *Accounts Chem Res* **2008**, *41*, 1215.

Hsu, T. J.; Fowler, F. W.; Lauher, J. W. *J Am Chem Soc* **2012**, *134*, 142.

Socrates, G. *Infrared and Raman characteristic group frequencies : tables and charts*; 3rd ed.; Wiley: Chichester, **2001**.

Xu, R.; Schweizer, W. B.; Frauenrath, H. *Chem-Eur J* **2009**, *15*, 9105.

Yoon, J.; Kim, J. M. *Macromol Chem Phys* **2008**, *209*, 2195.

Lifshitz, Y.; Golan, Y.; Konovalov, O.; Berman, A. *Langmuir* **2009**, *25*, 4469.

Cho, J. T.; Woo, S. M.; Ahn, D. J.; Ahn, K. D.; Lee, H.; Kim, J. M. *Chem Lett* **2003**, *32*, 282.

Jiang, H.; Pan, X. J.; Lei, Z. Y.; Zou, G.; Zhang, Q. J.; Wang, K. Y. *J Mater Chem* **2011**, *21*, 4518.

Cho, S.; Han, G.; Kim, K.; Sung, M. M. *Angew Chem Int Edit* **2011**, *50*, 2742.

Lee, S. B.; Koepsel, R.; Stolz, D. B.; Warriner, H. E.; Russell, A. J. *J Am Chem Soc* **2004**, *126*, 13400.

Yarimaga, O.; Yoon, B.; Ham, D. Y.; Lee, J.; Hara, M.; Choi, Y. K.; Kim, J. M. *J Mater Chem* **2011**, *21*, 18605.

Tabata, H.; Tokoyama, H.; Yamakado, H.; Okuno, T. *J Mater Chem* **2012**, *22*, 115.

Ellis, D. L. Z., M. R.; Bernstein, L. S.; Rubner, M. F *Polymeric Materials Science and Engineering* **1994**, *71*, 2.

Thomas, H. R.; Salaneck, W. R.; Duke, C. B.; Plummer, E. W.; Heeger, A. J.; Macdiarmid, A. G. *Polymer* **1980**, *21*, 1238.

Groenewoud, L. M. H.; Weinbeck, A. E.; Engbers, G. H. M.; Feijen, J. *Synthetic Met* **2002**, *126*, 143.

Li, J.; Rajca, A.; Rajca, S. *Synthetic Met* **2003**, *137*, 1507.

Sakamoto, M.; Wasserman, B.; Dresselhaus, M. S.; Wnek, G. E.; Elman, B. S.; Sandman, D. J. *J Appl Phys* **1986**, *60*, 2788.

Whelan, C. M.; Cecchet, F.; Baxter, R.; Zerbetto, F.; Clarkson, G. J.; Leigh, D. A.; Rudolf, P. *J Phys Chem B* **2002**, *106*, 8739.

Aldissi, M.; Armes, S. P. *Macromolecules* **1992**, *25*, 2963.

Zeng, X. R.; Ko, T. M. *J Polym Sci Pol Phys* **1997**, *35*, 1993.

Hsu, S. L.; Signorelli, A. J.; Pez, G. P.; Baughman, R. H. *J Chem Phys* **1978**, *69*, 106.

Grigorian, L.; Williams, K. A.; Fang, S.; Sumanasekera, G. U.; Loper, A. L.; Dickey, E. C.; Pennycook, S. J.; Eklund, P. C. *Phys Rev Lett* **1998**, *80*, 5560.